Neurobiology of Disease 139 (2020) 104808

Contents lists available at ScienceDirect

Neurobiology of Disease

journal homepage: www.elsevier.com/locate/ynbdi

Dynamic functional connectivity and graph theory metrics in a rat model of temporal lobe epilepsy reveal a preference for brain states with a lower functional connectivity, segregation and integration

Emma Christiaen[a,*], Marie-Gabrielle Goossens[b], Benedicte Descamps[a], Lars E. Larsen[a,b], Paul Boon[b], Robrecht Raedt[b,1], Christian Vanhove[a,1]

[a] MEDISIP, Department of Electronics and Information Systems, Ghent University, Ghent, Belgium
[b] 4Brain Team, Department of Head and Skin, Ghent University, Ghent, Belgium

ARTICLE INFO

Keywords:
Resting state functional MRI
Temporal lobe epilepsy
Intraperitoneal kainic acid rat model
Dynamic functional connectivity
Sliding window analysis

ABSTRACT

Epilepsy is a neurological disorder characterized by recurrent epileptic seizures. The involvement of abnormal functional brain networks in the development of epilepsy and its comorbidities has been demonstrated by electrophysiological and neuroimaging studies in patients with epilepsy. This longitudinal study investigated changes in dynamic functional connectivity (dFC) and network topology during the development of epilepsy using the intraperitoneal kainic acid (IPKA) rat model of temporal lobe epilepsy (TLE). Resting state functional magnetic resonance images (rsfMRI) of 20 IPKA animals and 7 healthy control animals were acquired before and 1, 3, 6, 10 and 16 weeks after status epilepticus (SE) under medetomidine anaesthesia using a 7 T MRI system. Starting from 17 weeks post-SE, hippocampal EEG was recorded to determine the mean daily seizure frequency of each animal. Dynamic FC was assessed by calculating the correlation matrices between fMRI time series of predefined regions of interest within a sliding window of 50 s using a step length of 2 s. The matrices were classified into 6 FC states, each characterized by a correlation matrix, using k-means clustering. In addition, several time-variable graph theoretical network metrics were calculated from the time-varying correlation matrices and classified into 6 states of functional network topology, each characterized by a combination of network metrics. Our results showed that FC states with a lower mean functional connectivity, lower segregation and integration occurred more often in IPKA animals compared to control animals. Functional connectivity also became less variable during epileptogenesis. In addition, average daily seizure frequency was positively correlated with percentage dwell time (i.e. how often a state occurs) in states with high mean functional connectivity, high segregation and integration, and with the number of transitions between states, while negatively correlated with percentage dwell time in states with a low mean functional connectivity, low segregation and low integration. This indicates that animals that dwell in states of higher functional connectivity, higher segregation and higher integration, and that switch more often between states, have more seizures.

1. Introduction

Functional magnetic resonance imaging (fMRI) is a neuroimaging technique that allows non-invasive visualisation of whole-brain activity. It detects changes in the blood oxygenation level dependent (BOLD) signal, which reflects neuronal activity (Matthews and Jezzard, 2004). Generally, fMRI is used to construct maps indicating brain regions that are activated by a certain task. In contrast to task-based fMRI, resting-state fMRI (rsfMRI) does not require subjects to perform any specific task. During rest, background activity modulates the BOLD signal, inducing spontaneous low frequency fluctuations. Based on statistical dependencies between the BOLD time series of brain regions of interest, functionally connected regions can be identified and functional brain networks can be detected (Wang et al., 2010). Several techniques can be used to assess functional connectivity, such as seed-based correlation, independent component analysis (ICA) and graph theory (Smitha et al., 2017). Functional connectivity is affected in several neurological disorders, including Alzheimer's disease, depression, schizophrenia, attention-deficit hyperactivity disorder and epilepsy (Fox and Greicius, 2010).

* Corresponding author.
E-mail address: emma.christiaen@ugent.be (E. Christiaen).
[1] Christian Vanhove and Robrecht Raedt should be considered joint senior author.

https://doi.org/10.1016/j.nbd.2020.104808
Received 11 December 2019; Received in revised form 21 January 2020; Accepted 18 February 2020
Available online 19 February 2020

In most rsfMRI studies, functional connectivity is calculated based on statistical dependencies between brain regions over the entire scan, which usually lasts 5 to 20 min, and is thus assumed to be stationary (Preti et al., 2017). However, several fMRI and electrophysiological studies have demonstrated that functional connectivity fluctuates within shorter time scales of seconds (Chang and Glover, 2010; Preti et al., 2017). To capture these fast changes, dynamic functional connectivity (dFC) can be used (Grandjean et al., 2017). The most common strategy to investigate dFC is using a sliding window approach where pairwise connectivity between brain regions or voxels is repeatedly evaluated for (non)overlapping time windows of data (Hutchison et al., 2013; Preti et al., 2017). Differences in dFC between patients and controls have been found in several neurological disorders, including schizophrenia, autism, mild cognitive impairment, Alzheimer's disease, post-traumatic stress disorder and multiple sclerosis (for review see Preti et al., 2017), but also in epilepsy (Klugah-Brown et al., 2019; Li et al., 2018a, 2018b; Liu et al., 2017; Pedersen et al., 2017; Wang et al., 2019).

Epilepsy is a neurological disorder characterized by recurrent epileptic seizures (Fisher et al., 2005) and about one third of patients suffer from drug-resistant epilepsy, i.e., their seizures cannot be controlled with anti-epileptic drugs. The most common type of acquired drug-resistant epilepsy is temporal lobe epilepsy (TLE) (Engel Jr, 2014). Using different analysis techniques, dFC studies found several alterations in TLE patients, including altered mean and variance of the BOLD signal (Laufs et al., 2014) and altered variability of functional connectivity and graph theory metrics (Chiang et al., 2018, 2016; Laufs et al., 2014; Morgan et al., 2015).

Epilepsy is often caused by an initial precipitating insult (IPI) such as stroke, infection, trauma, brain tumor or (febrile) status epilepticus (SE). Following an IPI, functional and structural changes occur in the brain which in some patients are associated with the development of spontaneous epileptic seizures. The process where a healthy brain is transformed into an epileptic brain is called epileptogenesis (Goldberg and Coulter, 2013).

In this study, changes in dynamic FC and network topology during the development of epilepsy were investigated in the intraperitoneal kainic acid (IPKA) rat model of TLE. The aim of this study was twofold: (1) to characterize how dFC and dynamic network topology of the rat brain change after SE and during the development of TLE, and (2) to evaluate whether these changes are associated with the occurrence of spontaneous seizures. To the best of our knowledge, no studies have investigated dFC and dynamic network topology in an animal model of epilepsy.

2. Materials and methods

2.1. Data set

The data set consisted of rsfMRI scans and EEG recordings of 27 adult male Sprague-Dawley rats (276 ± 15 g body weight; Envigo, The Netherlands), of which 20 were IPKA animals and 7 control animals. An extra data set was used to validate our methods. This validation data set consisted of rsfMRI scans of 8 adult male Sprague-Dawley rats (237 ± 11 g body weight; Envigo), all of which were IPKA animals.

2.2. Animals

The animals were treated according to European guidelines (directive 2010/63/EU). The local Ethical Committee on Animal Experiments of Ghent University (ECD 16/31) approved the protocol. The animals were housed individually in type III H cages (Tecniplast, Australia) on wood-based bedding (Carfil, Belgium), under environmentally controlled conditions (12 h normal light/dark cycles, 20–23 °C and 40–60% relative humidity) with food (Rats and Mice Maintenance, Carfil, Belgium) and water ad libitum. Paper nesting material (Nesting, Carfil, Belgium) and a gnawing wood (M-brick, Carfil, Belgium) were used to enrich the cages.

2.3. Status epilepticus

Twenty animals of the main data set and all 8 animals of the validation data set were intraperitoneally (i.p., 5 mg/kg/h) injected with kainic acid (KA; Tocris Bioscience, UK) according to the protocol of Hellier et al. (1998) at an age of 8 weeks. KA was administered every hour until motor seizures were elicited for at least 3 h, referred to as status epilepticus (SE). On average, the animals were injected with 12.7 mg/kg KA (range: 5–20 mg/kg). Two animals died during or within 4 h after SE induction. The other 7 animals of the main data set were injected similarly with saline and served as control group.

2.4. Image acquisition

In the main data set, anatomical and resting state functional MRI was performed one week before and 1, 3, 6, 10 and 16 weeks after SE. One IPKA rat was excluded 3 weeks after SE, because of a large artifact on the MR images caused by a metal fragment lodged behind its teeth. Anatomical and resting state functional MR images were acquired 20 weeks post-SE in the animals in the validation data set. These animals had been intrahippocampally injected with the viral vector AAV2/7-CamKIIα-hM4Di-mCherry (titer 2.78×10^{13} genome copies/ml) 16 weeks post-SE as part of an additional study. Animals were transported to the MR facility one day before scanning. They were sedated with medetomidine while the functional MR images were acquired (Weber et al., 2006). First, the animals were anesthetized with isoflurane (5% for induction, 2% for maintenance; Isoflo, Zoetis, USA) and O_2. Then a bolus of medetomidine (0.05 mg/kg; Domitor, Orion Pharma, Finland) was injected subcutaneously and after 10 min, isoflurane anaesthesia was discontinued. Continuous subcutaneous infusion of medetomidine (0.1 mg/kg/h) was started 15 min after the bolus injection and 25 min later functional MR images were acquired. Anaesthesia was reversed after the image acquisition with a subcutaneous injection of atipamezole (0.1 mg/kg; Antisedan, Orion Pharma, Finland). The MR images were acquired on a 7 T system (PharmaScan, Bruker, Germany) using a transmit body volume coil (Rapid Biomedical, Germany) and an actively decoupled rat head surface coil (Rapid Biomedical, Germany) to receive the signal. A circulating-water heating pad maintained the body temperature of the animals and respiration was measured using a pressure sensor. After optimizing the magnetic field homogeneity, TurboRARE T2-weighted anatomical images (TR: 3661 ms, TE: 37 ms, 30 slices, FOV: 35×35 mm^2, in-plane slice resolution: 109×109 μm^2, slice thickness: 0.6 mm, acquisition time: 9 min 46 s) were acquired. Next, 3 rsfMRI scans were acquired for the main data set and 2 for the validation data set using single-shot gradient echo echo-planar imaging (GE-EPI; TR: 2000 ms, TE: 20 ms, 16 slices, FOV: 30×30 mm^2 and voxel size: $0.375 \times 0.375 \times 1$ mm^3). Each rsfMRI scan consisted of 300 repetitions and lasted 10 min.

2.5. Electrode implantation

On average 19.5 weeks after SE (range 17 to 23 weeks), recording electrodes were implanted in both hippocampi in the animals of the main data set. The rats were anesthetized with a mixture of isoflurane (5% for induction, 2% for maintenance) and medical O_2. After exposing the skull, 13 small burr holes were drilled: 9 for positioning of stainless steel anchor screws (1.75 mm diameter; PlasticsOne, USA), 2 for the epidural ground/reference electrodes above right and left frontal cortex respectively and 2 for bilateral hippocampal EEG recording electrodes. Epidural electrodes and bipolar recording electrodes were custom-made by connecting an insulated copper wire to an anchor screw and by twisting two polyimide-coated stainless steel wires (70 μm bare diameter, 900 μm distance between wire tips; California Fine Wire, USA)

around each other, respectively. Recording electrodes were implanted in the left and right hippocampus using stereotactic coordinates based on the Rat Brain Atlas by Paxinos and Watson (2013) (AP -3.8 mm, ML ± 2.2 mm relative to bregma, DV about −3.3 mm relative to brain surface). The T2-weighted anatomical MR images, obtained 16 weeks post-SE, were used to check whether the implantation site was free of KA-induced lesions. Real time electrophysiological recordings were monitored visually and auditively during positioning of the electrodes to ensure that one tip of the electrode was placed in the subgranular layer of the dentate gyrus and the other in the pyramidal cell layer of the CA1 region. All electrode leads ended in a connector that was attached to the skull and the anchor screws using acrylic dental cement. Meloxicam (1 mg/kg, subcutaneously, Boehringer Ingelheim, Germany) was injected at the end of the surgery and lidocaine (2% Xylocaine gel, AstraZeneca, UK) was locally applied to the wound to minimize discomfort. Meloxicam was injected a second time 24 h after surgery.

2.6. EEG recording

EEG recordings were started after one to two weeks of recovery. The EEG set up consisted of a custom-built head stage with unity gain preamplifier (based on TI TL074 JFET OpAmps), shielded 12-channel cables (363/2-000; PlasticsOne), a 12-channel commutator (SL12C; PlasticsOne) and a custom-built 512× amplifier (based on TI TL074 JFET OpAmps and a first order high-pass filter with a time constant of 1 s). Animals were awake and freely moving during the recording period. Signals were sampled at 2 kHz by a 16-bit resolution data acquisition card (USB-6259, National Instruments, USA) and stored on the computer for offline analysis by a Matlab-based script (MathWorks, USA). Experienced investigators annotated seizures visually. An electrographic seizure was defined as a repetitive pattern (> 2 Hz) of complex, high amplitude EEG spikes that lasts for minimally 5 s. Following an acclimatization period of 3 days, average number of seizures per day was calculated based on 7 consecutive days of EEG recording.

2.7. Dynamic functional brain network

2.7.1. Parcellation

An in-house parcellated atlas containing 38 cortical and subcortical regions of interest (ROIs), manually constructed based on T2w anatomical images of part of the main data set (10 animals) using SPM12 (https://www.fil.ion.ucl.ac.uk/spm/software/spm12/) and Matlab, was used to construct the dynamic functional brain network. The ROIs included auditory cortex, caudate putamen, cingulate cortex, dorsolateral orbital cortex, globus pallidus, hippocampus, insula, motor cortex, nucleus accumbens, parietal association cortex, piriform cortex, posterior parietal cortex, prelimbic cortex, retrosplenial cortex, septum, somatosensory cortex, temporal association cortex, thalamus and visual cortex, each in the left and right hemisphere. The atlas was adapted to the IPKA model, i.e., hyperintensities visible on the T2w images indicative for structural damage were excluded from the ROIs.

2.7.2. Sliding window analysis

The sliding window approach, implemented in the Graph Theoretical Network Analysis (GRETNA; Wang et al., 2015) toolbox, was used to calculate the dFC between the ROIs (Fig. 1). The mean time series for each ROI were extracted and the Pearson correlation coefficient was calculated between each pair within a rectangular time window of 50 s. Then the time window was shifted repeatedly with 2 s and each time the correlation coefficients were calculated. This way 276 correlation matrices (38 × 38) were obtained for each scan. For further analysis, the correlation coefficients were Fisher r-to-z transformed to obtain a normal distribution. In addition, graph theory was used to assess the functional organization of the brain within each time window (Rubinov and Sporns, 2010). The correlation matrices were represented as a graph with the ROIs as nodes and the correlation coefficients between the ROIs as edges. The weakest edges were removed to obtain a 35% network density, i.e., the number of remaining connections divided by the maximum number of possible connections. Several graph theoretical metrics were calculated using GRETNA. On a global level, degree, characteristic path length, global efficiency, clustering coefficient and local efficiency were determined, and degree was calculated for each node or ROI as well. Degree is the number of edges connected to a node. Characteristic path length is the average number of edges connecting two nodes in the graph and global efficiency is the average inverse path length between two nodes. Clustering coefficient is the proportion of neighbours of a node that are also connected to one another, and local efficiency is global efficiency calculated within the neighbourhood of a node, i.e., the nodes connected to that node. Degree is a measure of the importance of a node in the graph, characteristic path length and global efficiency are measures of functional integration or overall communication efficiency, and clustering coefficient and local efficiency are measures of functional segregation or local interconnectivity in the network (Rubinov and Sporns, 2010; Wang et al., 2010).

2.8. States of functional connectivity and functional network topology

The correlation matrices were classified into a subset of connectivity states. These states can be seen as recurring patterns of functional connectivity. A k-means clustering algorithm (*kmeans* function in Matlab) was used to partition the correlation matrices into a number of clusters and the optimal number of clusters was determined by the Elbow method (Ketchen and Shook, 1996). In k-means clustering, the total intra-cluster variation is minimized. The Elbow method calculates the intra-cluster variation in function of the number of clusters and determines for which number of clusters, adding another cluster does not lead to a large decrease in intra-cluster variation. The clustering was performed on the entire data set containing 144,900 correlation matrices, consisting of the scans of all animals of the main data set at all time points. For each state of functional connectivity, mean, standard deviation, maximum and minimum z-scores were calculated. Then they were sorted from highest to lowest mean value. In addition, the graph theoretical network metrics characteristic path length, clustering coefficient, global and local efficiency, and global and nodal degree were calculated for each state. These network metrics were calculated at different densities of the correlation matrices, from 20% to 50% density with a 5% interval, and averaged over these densities. Moreover, coreness of the nodes was used to assess the importance of the nodes in each functional connectivity state, regardless of the mean value of this state. A functional brain network usually consists of a core, i.e., a set of highly connected nodes, and a periphery, i.e., the other, weakly connected, nodes. Coreness indicates how often a node is part of the core and is a number between 0 (never in the core) and 1 (always in the core) (Battiston et al., 2018). To calculate coreness, all nodes are ranked from highest to lowest degree. Then the connection strength with all nodes with a higher degree is calculated for each node. The node for which this value is maximal is the limit of the core. All nodes with a higher degree are part of the core and are assigned coreness 1, all nodes with a lower degree are part of the periphery and are assigned coreness 0. This is done for all network densities and averaged, leading to a coreness between 0 and 1 for each node in the network.

To assess the variability in functional network topology, the standard deviation over the 276 time windows was calculated for all graph theoretical network metrics. Then, the time-varying network topology, characterized by a combination of the global network metrics degree, clustering coefficient, characteristic path length and local and global efficiency, was classified into a subset of states as well.

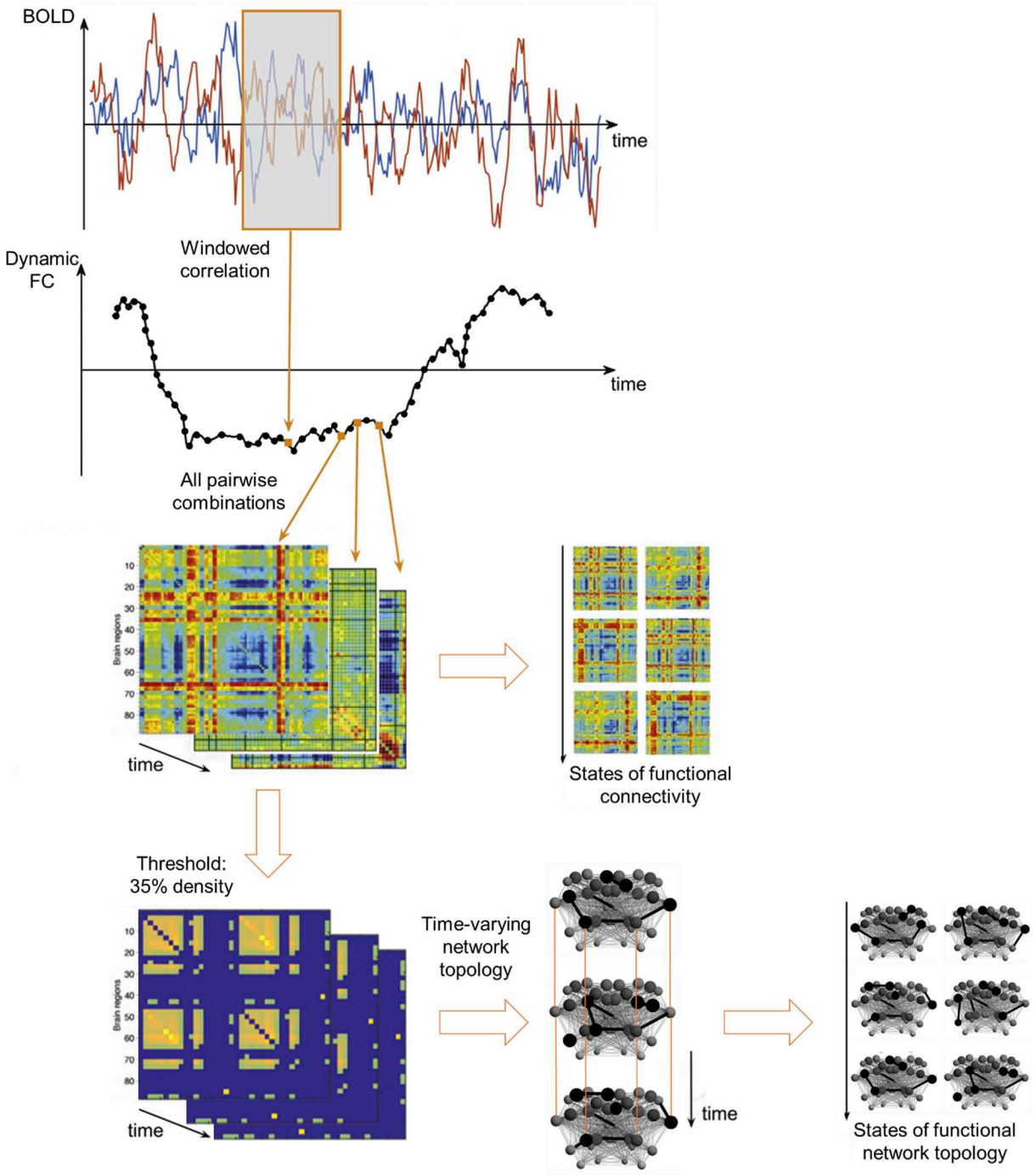

Fig. 1. Construction and clustering of dynamic functional brain networks: Pearson correlation coefficient is calculated between each pair of ROIs within a rectangular time window of 50 s that is shifted repeatedly with 2 s, to obtain 276 38 × 38 correlation matrices that are then clustered into 6 recurring states of functional connectivity. After applying a threshold to obtain a network density of 35%, several graph theoretical network metrics are calculated for each correlation matrix to quantify its topology. The different network topologies are then clustered into 6 states of functional network topology (Adapted from Preti et al., 2017).

2.9. Dwell time and number of transitions

For each animal and each time point, the percentage dwell time for each state of functional connectivity and network topology was determined. This was calculated as the ratio of the number of times a state occurs within a scan to the total number of windows within the scan (n = 276). In addition, the number of transitions was calculated. This is the number of times the functional connectivity changes between states within a scan, i.e., within 10 min. These parameters, and the variability in network topology, were statistically analysed using a linear mixed-effects model (LMEM) in IBM SPSS Statistics for Windows, version 26 (IBM Corp., N.Y., USA). The covariance structure was the 'compound symmetry' structure, fixed factors were group (IPKA animals and control animals), time (baseline, 1, 3, 6, 10 and 16 weeks after SE) and group-by-time interaction. Least-significant-difference tests were used to explore significant effects and interactions, a significance level of 0.05 was used for main effects and interactions, and the Bonferroni and false discovery rate (FDR) correction were used to correct for multiple comparisons between time points and variables, respectively. For some parameters, the assumption of normally distributed residuals was not

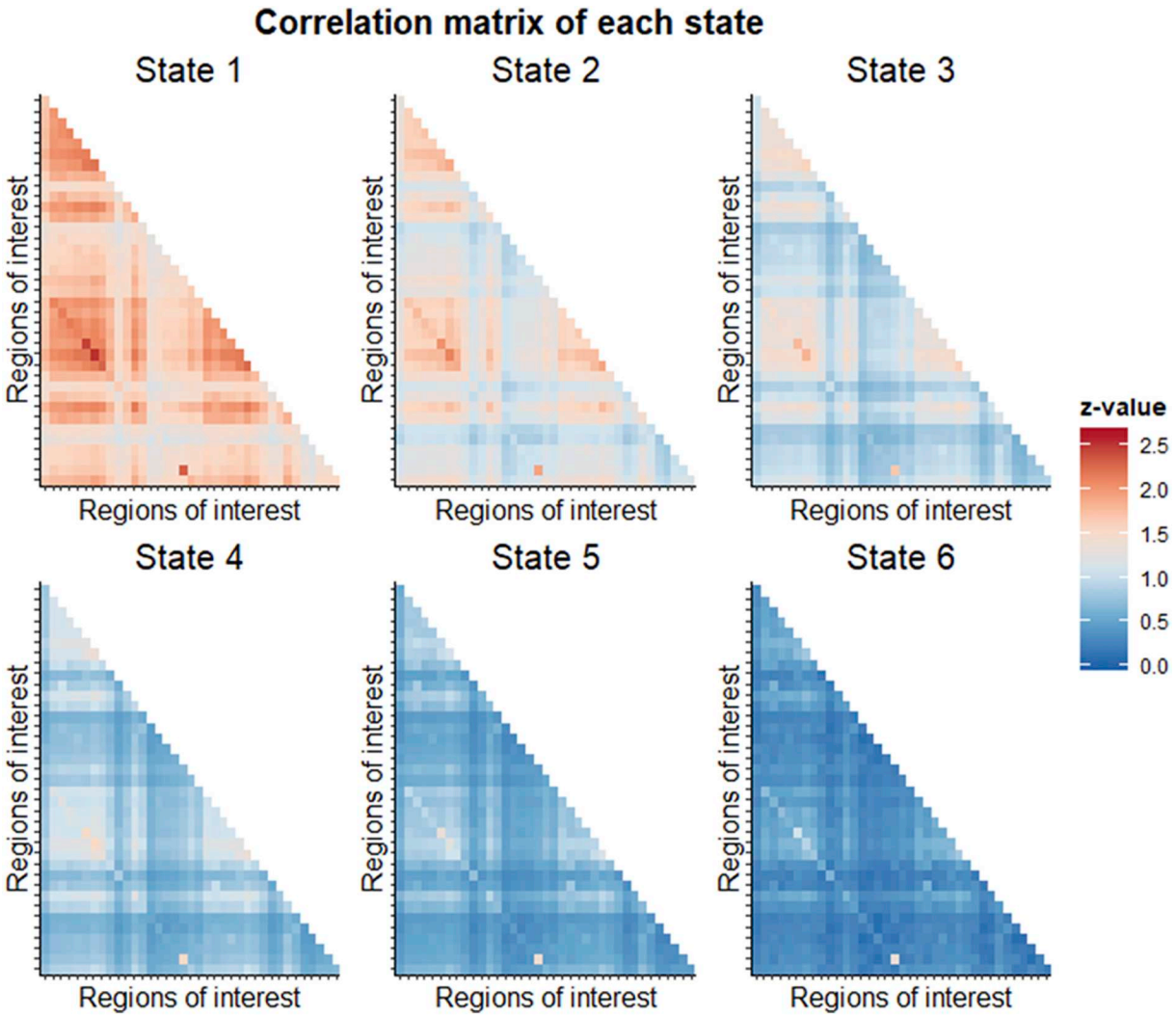

Fig. 2. Correlation matrices (z-score) of 6 recurring states of functional connectivity, sorted from highest (State 1) to lowest (State 6) mean value.

Table 1
Characterization of 6 recurring states of functional connectivity determined using k-means clustering.

	State 1	State 2	State 3	State 4	State 5	State 6
Mean	1.65	1.28	1.03	0.80	0.58	0.35
Standard deviation	0.24	0.24	0.22	0.21	0.18	0.14
Maximum	2.53	2.11	1.81	1.55	1.42	1.35
Minimum	1.13	0.80	0.61	0.42	0.26	0.08

met, most likely due to a large number of zero values in some states. In this case, effect of group was evaluated using the non-parametric Mann-Whitney *U* test and effect of time with the non-parametric Friedmann test. For pairwise comparisons, the Mann-Whitney U test and Wilcoxon signed-rank test were used for between-group and within-group statistical testing, respectively, and the Bonferroni correction was used to correct for multiple comparisons.

2.10. Correlation with seizure frequency

The Pearson correlation coefficient was calculated to assess the correlation between mean daily seizure frequency and dFC parameters such as dwell time in states of functional connectivity and network topology, number of transitions between states, and standard deviation of global network metrics at each time point. A significance level of 0.05 was used. If the one-sample Kolmogorov-Smirnov test showed that one of the variables was not normally distributed, Spearman's rank-order correlation was used instead of Pearson correlation. FDR correction was used to correct for multiple comparisons when calculating the correlation between seizure frequency and percentage dwell time in different states at the same time point.

2.11. Influence of window length

One of the limitations of a sliding window analysis, is that the window length has to be chosen a priori. If it is too short, false fluctuations can be observed in the dFC, but if the window length is too long, not all genuine fluctuations will be detected. A window length of 30 to 60 s is usually a good trade-off (Preti et al., 2017). In this study, we chose a window length of 50 s or 25 TRs. To assess the influence of the choice of window length, we repeated the calculation of dwell time in and number of transitions between states of functional connectivity using window lengths of 30 s (15 TRs) and 70 s (35 TRs).

2.12. Validation of epileptic dynamic functional connectivity

An extra data set was used to validate our results. This data set consisted of rsfMRI scans in 8 IPKA animals, acquired 20 weeks post-SE. The dynamic functional brain network was constructed using the parcellated atlas of the main data set and a sliding window length of 50 s.

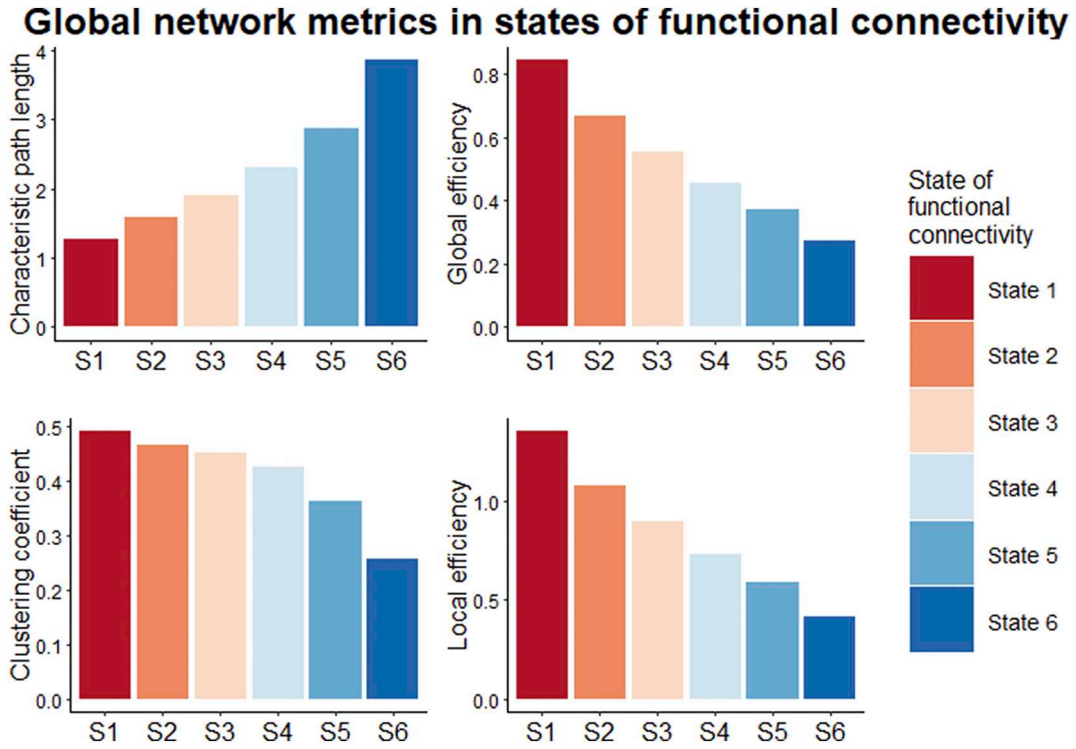

Fig. 3. Global network metrics for each state of functional connectivity. Characteristic path length increases from State 1 to State 6, while clustering coefficient and local and global efficiency decrease.

Each correlation matrix was assigned to one of the states of FC of the main data set using the Matlab function *pdist2*. This function determines which FC state is the closest match to each matrix based on Euclidian distance. Again, percentage dwell time in each state and number of transitions were calculated. Then, a two-sample Kolmogorov-Smirnov test assessed whether these parameters came from the same distribution as those of the IPKA group in the main data set.

3. Results

3.1. States of functional connectivity and network topology

Using k-means clustering and the Elbow method, all time-varying correlation matrices were assigned to one of 6 recurring states of functional connectivity (Fig. 2). For each state, mean, standard deviation, maximum and minimum z-scores are listed in Table 1. The states were sorted from highest (State 1) to lowest mean value (State 6). In addition, 4 global network metrics were calculated and displayed in Fig. 3. Characteristic path length was lowest in State 1 and highest in State 6, while clustering coefficient and local and global efficiency were highest in State 1 and lowest in State 6. In Fig. 4, nodal degree and coreness are visualized for each state. Average degree decreased from State 1 to State 6, but the relative importance of the nodes in the network remained similar. For each state, the core consisted of somatosensory cortex, cingulate cortex, motor cortex, visual cortex, caudate putamen, thalamus, retrosplenial cortex and hippocampus. Of these regions, visual cortex, thalamus and hippocampus varied most between states.

Network metrics were not only calculated for the 6 FC states, but also for the time-varying correlation matrices. The standard deviation over the 276 time windows of global degree, clustering coefficient and global efficiency is visualized in Fig. 5. Statistical analysis showed that standard deviation of global degree and global efficiency was significantly lower in the IPKA group compared to the control group ($U = 1.27\ 10^3$, $p < .001$ and $U = 1.21\ 10^3$, $p < .001$, respectively), while standard deviation of clustering coefficient was significantly higher ($F_{1,24.3} = 12.5$, $p = .002$). Standard deviation of global degree and global efficiency decreased significantly during epileptogenesis in the IPKA group ($\chi^2 = 22.3$, $p < .001$ and $\chi^2 = 15.6$, $p = .008$, respectively) but not in the control group ($\chi^2 = 1.61$, $p = .900$ and $\chi^2 = 3.08$, $p = .687$, respectively). There was a significant increase in standard deviation of clustering coefficient during epileptogenesis in the IPKA group ($F_{5,123} = 3.93$, $p = .002$), but not in the control group ($F_{5,122} = 1.45$, $p = .210$).

The time-varying network metrics were also decomposed into 6 recurring states of functional network topology using k-means clustering in combination with the Elbow method. The states were sorted from highest to lowest global degree. Clustering coefficient, local and global efficiency were highest in State 1 and lowest in State 6, while characteristic path length was lowest in State 1 (Fig. 6).

3.2. Percentage dwell time in states of functional connectivity and network topology

Percentage dwell time was calculated for each state of functional connectivity and network topology and visualized as a function of time, i.e., the number of weeks post-SE, for the IPKA group and the control group. In Fig. 7, each segment of a bar represents the percentage dwell time in a state averaged over the animals in the group (IPKA group or control group) at one time point. The 6 states always add up to 100%. Statistical analysis revealed a significant difference in percentage dwell time between the control and IPKA group. The dwell time in State 1, 2 and 3 was significantly lower in the IPKA group compared to the control group, while dwell time in State 5 and 6 was significantly higher in the IPKA group. A significant effect of time could be found in the IPKA group. There was a significant decrease in dwell time in State 1, 2, 3 and 4 and an increase in dwell time in State 5 and 6 during epileptogenesis in the IPKA group. No significant changes over time were found in the control group.

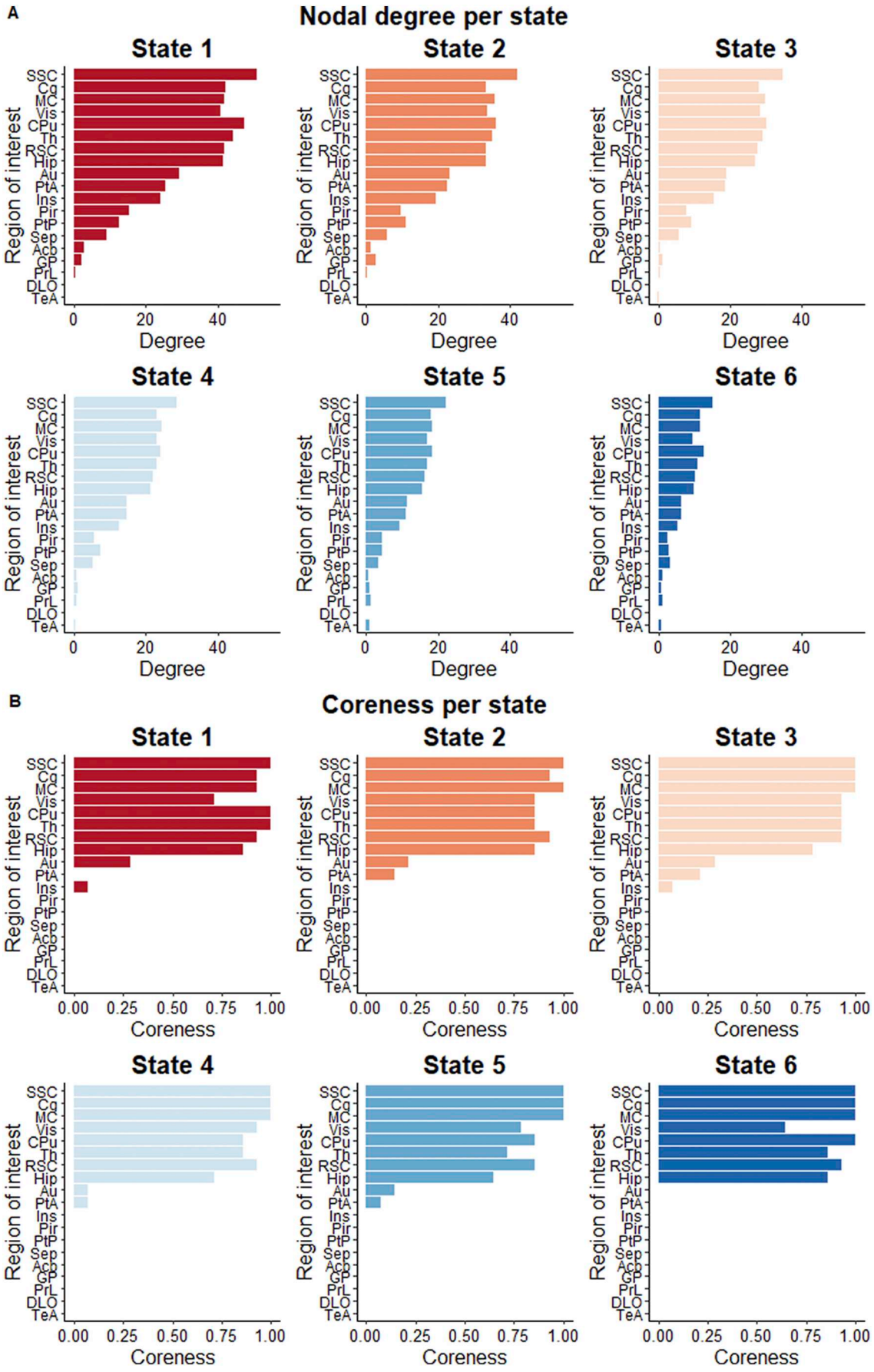

Fig. 4. A) Nodal degree and B) coreness for each state. On average, degree decreases from State 1 to State 6, but the relative importance of the nodes in the network remains similar. Data are visualized as a bar graph with mean values.

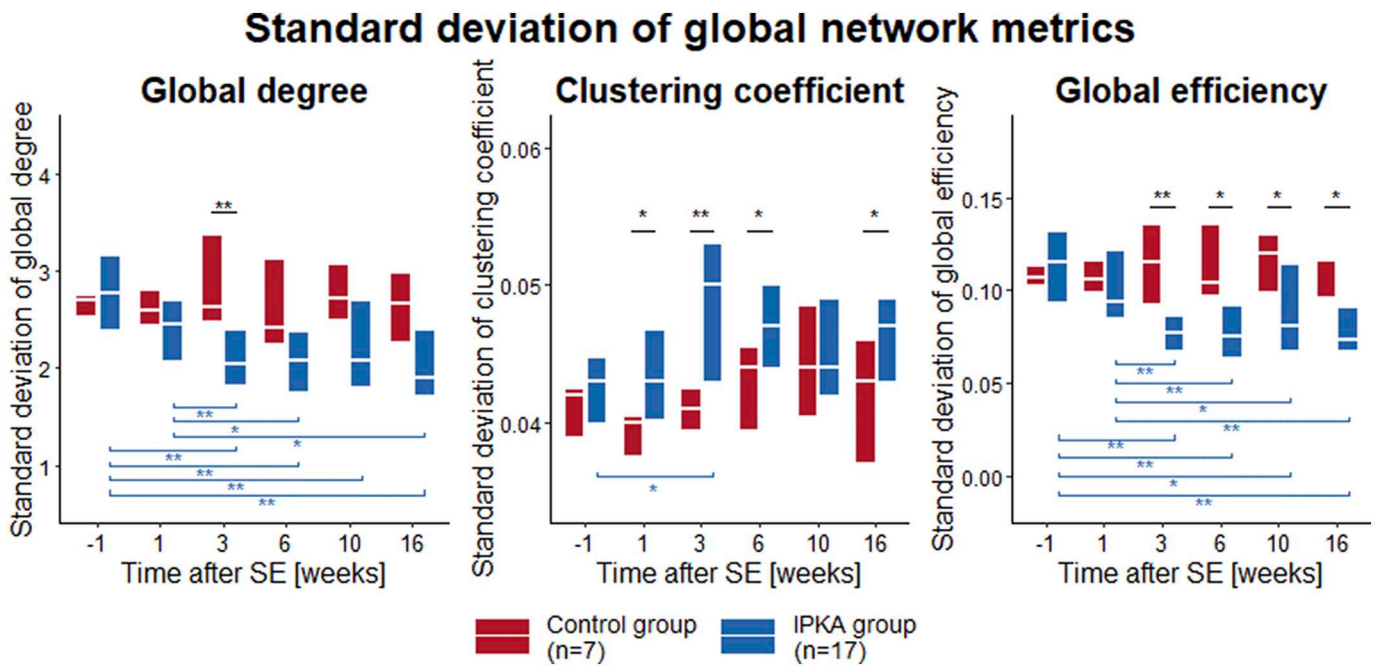

Fig. 5. Standard deviation over 276 time windows for global degree, clustering coefficient and global efficiency. Data are presented as a boxplot with median and interquartile range, $*p < .05$, $**p < .01$, $***p < .001$.

Similar results were obtained for percentage dwell time in states of functional network topology. In State 1, 2 and 3, dwell time was significantly lower in the IPKA group compared to the control group, while in State 5 and 6, dwell time was significantly higher in the IPKA group. Percentage dwell time in State 1, 2, 3 and 4 decreased significantly during epileptogenesis in the IPKA group, while it increased significantly in State 5 and 6. No significant changes over time were found in the control group. The results of the statistical analysis are summarized in Table 2.

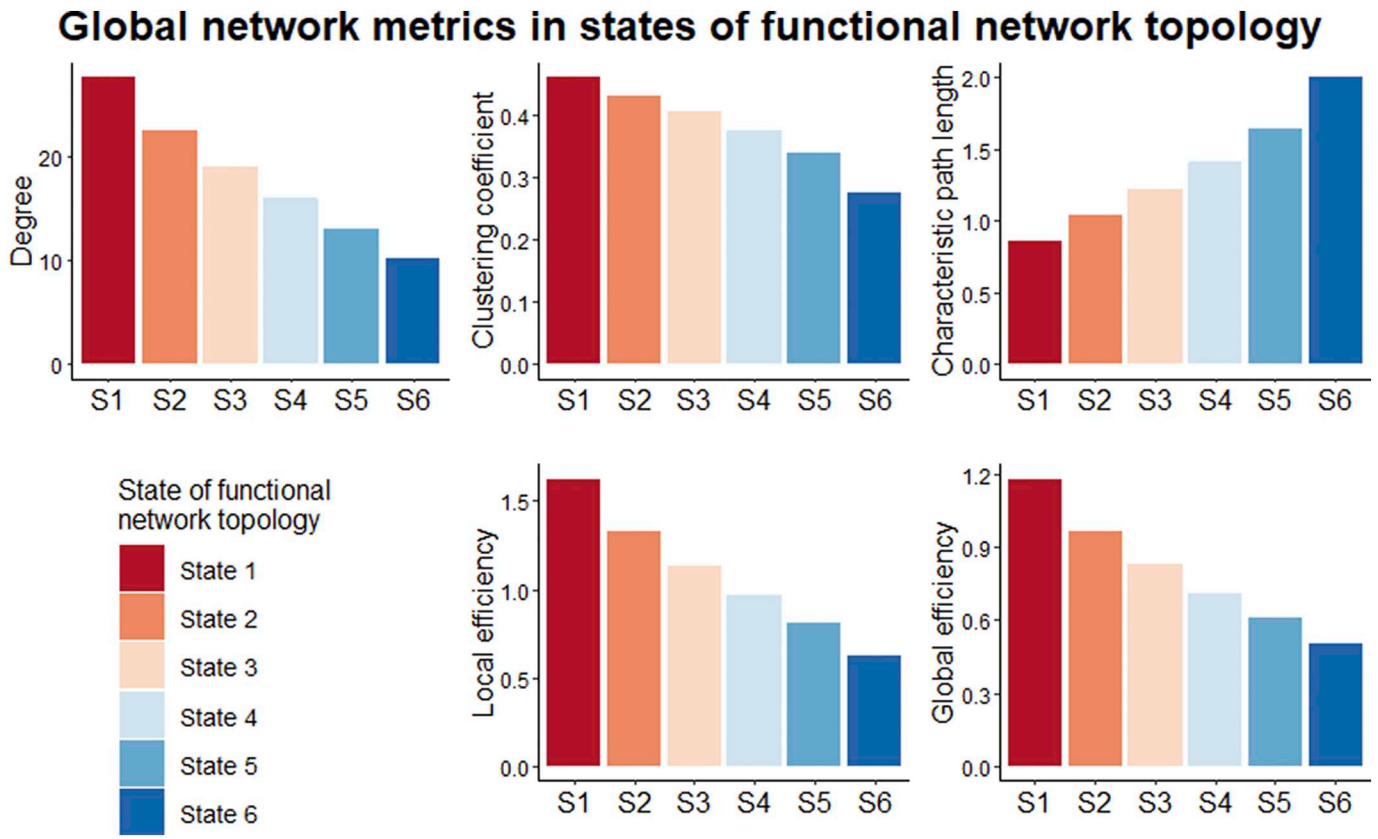

Fig. 6. Global network metrics for each state of functional network topology. Degree, clustering coefficient, local and global efficiency decrease from State 1 to State 6, while characteristic path length increases.

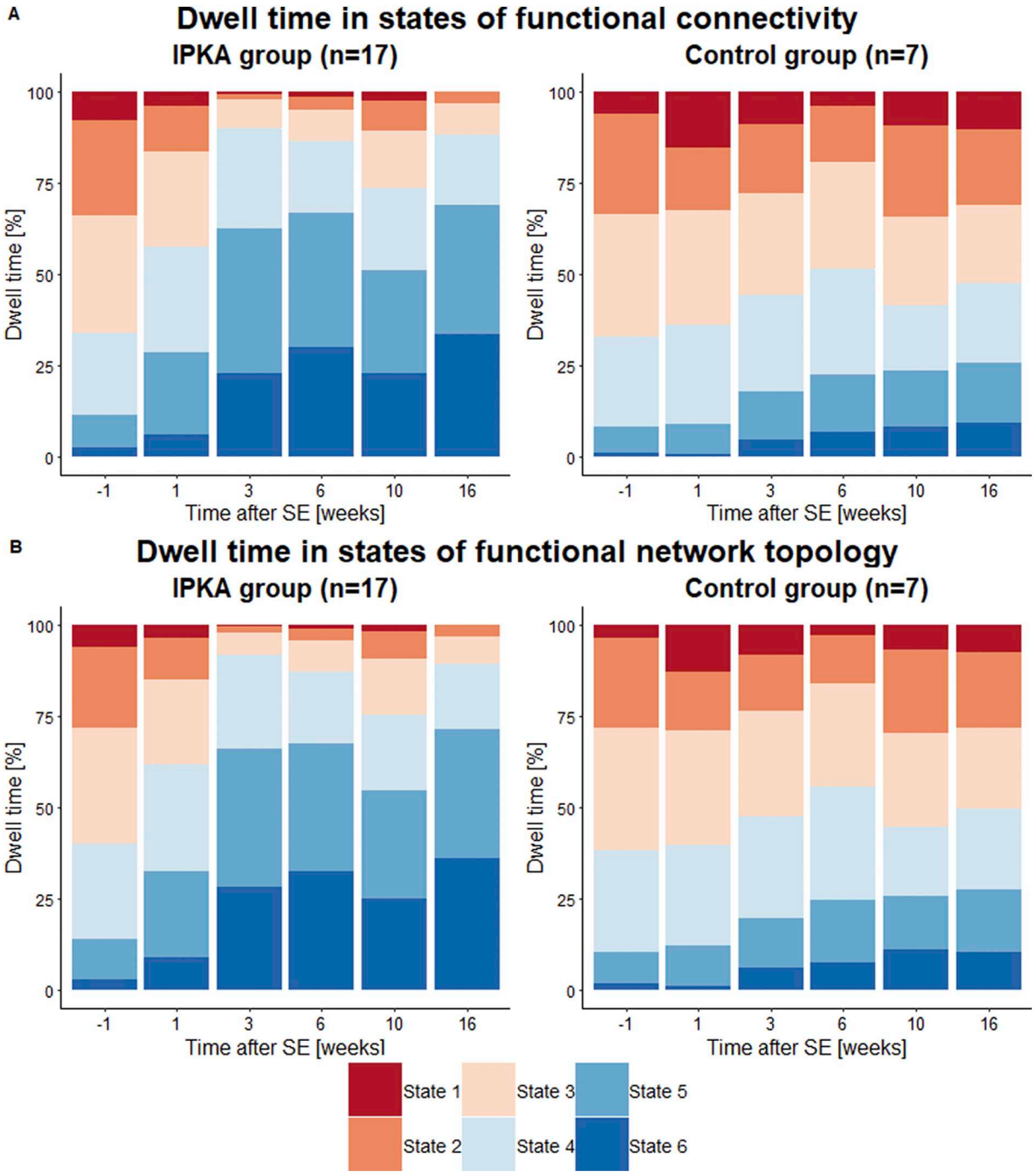

Fig. 7. Percentage dwell time in states of A) functional connectivity and B) functional network topology, visualized as a function of time (weeks post-SE) for the IPKA group and the control group. Data are visualized as a stacked bar graph with mean values. Each segment of a bar represents the percentage dwell time in a state averaged over the animals in the group at one time point. The 6 segments always add up to 100%.

3.3. Number of transitions between states of functional connectivity and network topology

The number of transitions between states of functional connectivity and states of functional network topology are visualized in Fig. 8A and B, respectively. Each stacked bar represents the total number of transitions at one time point averaged over all animals within one group (IPKA group or control group). Each segment of a bar represents the number of transitions between two specific states. Only transitions between consecutive states are represented, since transitions between non-consecutive states were rare.

The total number of transitions between states of functional connectivity was significantly lower in the IPKA group compared to the control group and decreased significantly during epileptogenesis in the IPKA group. More specifically, the number of transitions between states 1 and 2, 2 and 3, and 3 and 4 was significantly lower in the IPKA compared to the control group and decreased significantly during epileptogenesis in the IPKA group. The number of transitions between states 5 and 6 was significantly higher in the IPKA group and the number of transitions between states 4 and 5, and 5 and 6 increased significantly during epileptogenesis in the IPKA group.

Similar results were obtained for the number of transitions between states of functional network topology. The total number of transitions was significantly lower in the IPKA group compared to the control

Table 2
Results of statistical analysis of percentage dwell time in states of functional connectivity and network topology, *p*-values are FDR-corrected for multiple comparisons.

Dwell time		Effect of group		Effect of time IPKA group		Effect of time control group	
States of functional connectivity	State 1	$U = 1.29\ 10^3$	$p < .001$	$X^2 = 28.5$	$p < .001$	$X^2 = 3.39$	$p = .768$
	State 2	$U = 1.20\ 10^3$	$p < .001$	$X^2 = 36.1$	$p < .001$	$X^2 = 3.96$	$p = 1.00$
	State 3	$F_{1,26.0} = 14.6$	$p = .001$	$F_{5,125} = 17.7$	$p < .001$	$F_{5,123} = 1.22$	$p = 1.00$
	State 4	$U = 2.14\ 10^3$	$p = .724$	$X^2 = 11.1$	$p = .050$	$X^2 = 5.78$	$p = .987$
	State 5	$F_{1,26.0} = 16.9$	$p = .001$	$F_{5,124} = 16.9$	$p < .001$	$F_{5,123} = 0.780$	$p = .849$
	State 6	$U = 3.23\ 10^3$	$p < .001$	$X^2 = 37.5$	$p < .001$	$X^2 = 2.57$	$p = .766$
States of functional network topology	State 1	$U = 1.45\ 10^3$	$p < .001$	$X^2 = 30.5$	$p < .001$	$X^2 = 3.66$	$p = 1.00$
	State 2	$U = 1.16\ 10^3$	$p < .001$	$X^2 = 35.2$	$p < .001$	$X^2 = 2.88$	$p = 1.00$
	State 3	$F_{1,24.8} = 16.4$	$p = .001$	$F_{5,122} = 15.6$	$p < .001$	$F_{5,121} = 0.940$	$p = 1.00$
	State 4	$F_{1,25.0} = 0.692$	$p = .413$	$F_{5,122} = 2.70$	$p = .024$	$F_{5,122} = 1.16$	$p = 1.00$
	State 5	$F_{1,24.4} = 17.0$	$p = .001$	$F_{5,122} = 12.6$	$p < .001$	$F_{5,121} = 0.537$	$p = .898$
	State 6	$U = 1.14\ 10^3$	$p < .001$	$X^2 = 35.6$	$p < .001$	$X^2 = 2.19$	$p = .822$

group, but there was no significant effect of time in either group. In the IPKA group, the number of transitions between states 1 and 2, 2 and 3, and 3 and 4 was significantly lower and between states 5 and 6 significantly higher compared to the control group. There was a significant decrease in number of transitions between states 1 and 2, 2 and 3, and 3 and 4 during epileptogenesis in the IPKA group, while number of transitions between states 5 and 6 increased significantly. The results of the statistical analysis are summarized in Table 3.

3.4. Correlation of mean global network metrics, percentage dwell time and number of transitions with seizure frequency

During 7 days of consecutive EEG monitoring at least 19 weeks post-SE, the animals had a mean average daily seizure frequency of 22 seizures per 24 h (range: 0–53). One animal did not display any seizures on EEG during the recording period but did display occasional tonic-clonic seizures outside the recording period (e.g., when entering the housing room) and interictal epileptiform activity, such as epileptic spikes and pathological high frequency oscillations that could be observed on the EEG signal. Therefore, it was considered epileptic.

Seizure frequency was positively correlated with dwell time in the 2 higher states of functional connectivity one week post-SE, dwell time in State 4 16 weeks post-SE, and total number of transitions between states of functional connectivity 16 weeks post-SE. Seizure frequency was negatively correlated with dwell time in State 5 of functional connectivity one week post-SE and State 6 of functional connectivity 16 weeks post-SE (Fig. 9).

Seizure frequency was also positively correlated with dwell time in the 3 higher states of functional network topology (State 1, 2 and 3) one week post-SE, but negatively correlated with dwell time in State 5 of functional network topology. Sixteen weeks post-SE, dwell time in State 4 and 6 of functional network topology were positively and negatively correlated with seizure frequency, respectively. At this time point, seizure frequency was positively correlated with the total number of transitions between states as well (Fig. 10).

In addition, there was a positive correlation between average seizure frequency and the standard deviation over 276 time windows of global degree and local efficiency 1 week post-SE.

3.5. Influence of window length

Six states of functional connectivity were calculated using window lengths of 30 s (15 TRs) and 70 s (35 TRs). The mean value, standard deviation, maximum and minimum of each state for each window length were similar for the different window lengths (Fig. A.1, Table A.1). Similar changes in percentage dwell time and number of transitions were found for window lengths of 30 s and 70 s as for 50 s (Fig. A.2, Table A.2). The different window lengths resulted in a similar correlation of percentage dwell time and number of transitions with average daily seizure frequency (Table A.3).

3.6. Validation of epileptic dynamic functional connectivity

A two-sample Kolmogorov-Smirnov test could not demonstrate a significant difference between the percentage dwell time in each state and number of transitions of the validation data set and those of the main data set (Table 4, Fig. 11).

4. Discussion

4.1. Dwelling in states with a lower mean functional connectivity, segregation and integration

The aim of this study was to identify changes in dynamic functional connectivity and functional network topology during the development of epilepsy in the IPKA rat model of TLE, and to investigate whether these changes are associated with the occurrence of spontaneous seizures. In IPKA and control animals, 6 recurring states of functional connectivity could be distinguished. Percentage dwell time in the states with the highest mean functional connectivity was lower in the IPKA group compared to the control group, while dwell time was higher in the states with the lowest mean functional connectivity. In states with a higher mean functional connectivity, clustering coefficient and local efficiency were higher as well, indicating a high segregation or local interconnectivity. In these states, characteristic path length was lower and local efficiency higher, indicating a high integration or overall communication efficiency. Similarly, segregation and integration were lower in states with a lower mean functional connectivity. The decomposition of time-varying global graph theoretical network metrics into states of functional network topology led to similar results. Dwell time was lower in states with a higher functional connectivity, segregation and integration in the IPKA animals.

Significant changes in percentage dwell time could already be found 1 week post-SE, but the largest changes occurred between 1 and 3 weeks post-SE, after which dwell time remained constant. This timeline corresponds with the timing of structural changes during epileptogenesis in the IPKA rat model for TLE. During the first 4 weeks post-SE, neuronal degeneration can be found in hippocampus, amygdala, thalamus, piriform cortex and cortex and there is an increase in astrogliosis. Microgliosis already reaches a maximum 1 week post-SE, after which it remains high (Bertoglio et al., 2017; Sharma et al., 2008).

Our results indicate that the epileptic rat brain is characterized by states with a lower overall functional connectivity, segregation and integration, which is in line with studies investigating static functional connectivity in rat models of TLE. Christiaen et al. (2019) found a decreased functional connectivity, segregation and integration in the IPKA rat model for TLE, mainly in regions of the default-mode network (DMN). In the same model, Pirttimäki et al. (2016) reported small changes in functional connectivity in several brain regions 1 week post-SE and decreased functional connectivity, predominantly between the somatosensory cortex and thalamus and between the perirhinal and

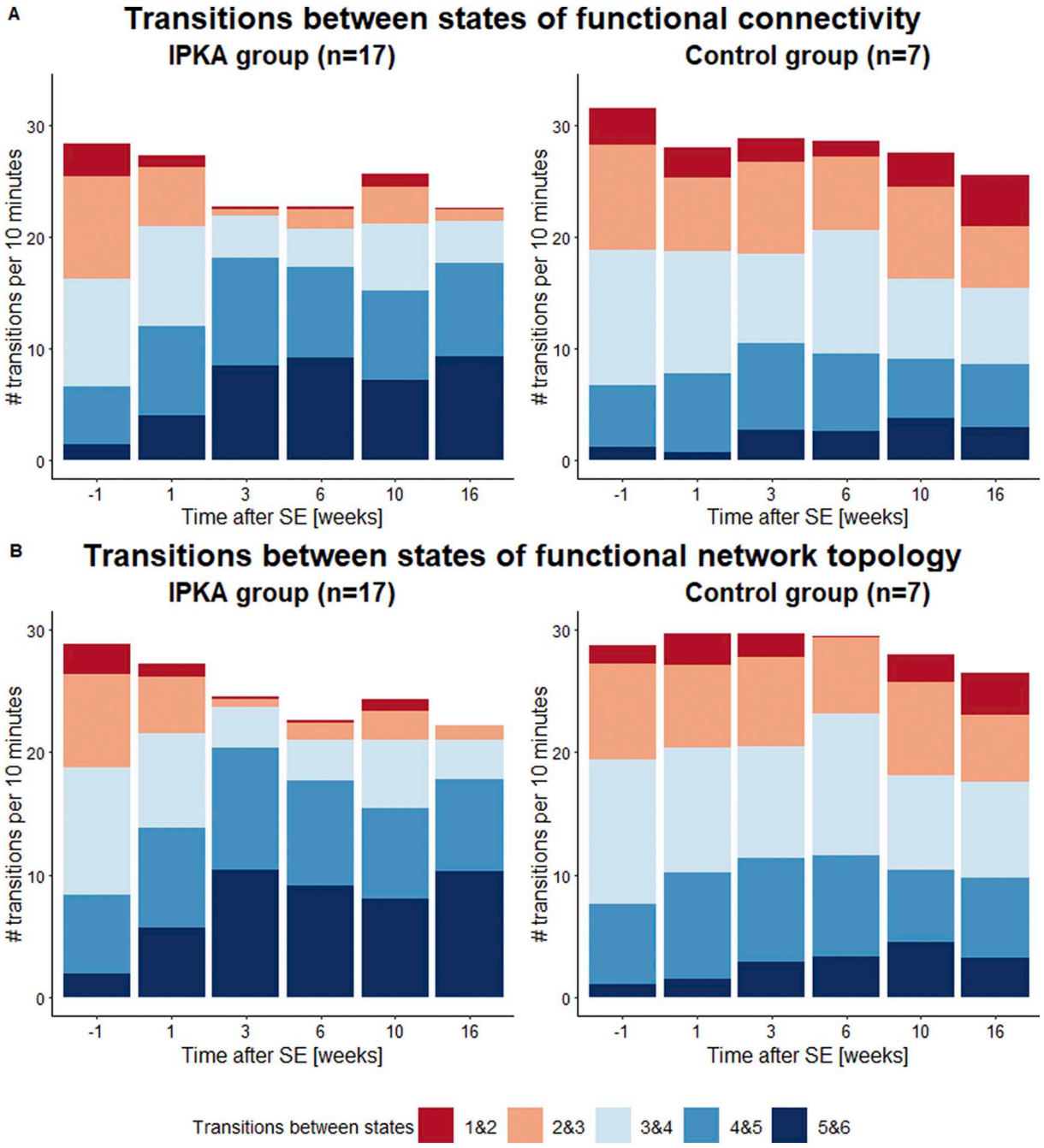

Fig. 8. Number of transitions between states of A) functional connectivity and B) functional network topology, visualized as a function of time (weeks post-SE) for the IPKA group and the control group. Data are visualized as a stacked bar graph with mean values. Each segment of a bar represents the number of transitions between 2 specific states averaged over the animals in the group at one time point.

piriform cortices, 1 or 2 months after SE. Bertoglio et al. (2019) demonstrated a highly affected functional connectivity in multiple regions of the DMN and a wide-spread network connectivity hyposynchrony 2 weeks post-SE. On the other hand, Gill et al. (2017) found that functional connectivity was increased within the temporal regions and the limbic network and between the anterior and posterior DMN 4 to 5 weeks post-SE. Jiang et al. (2018) demonstrated that connectivity of the hippocampal functional network was decreased in several regions, including hippocampus, amygdala, thalamus, motor cortex and somatosensy cortex, and increased in the visual cortex, mesencephalon and insula in the pilocarpine rat model of TLE. Overall, most of these studies found a decreased static functional connectivity in rat models of TLE. This is in agreement with our current findings regarding global changes in dynamic functional connectivity and network topology during epileptogenesis. In addition, it is in line with our finding that coreness, a measure for the relative importance of a node in the network, varies most between FC states in visual cortex, thalamus and hippocampus, 3 regions of the rat DMN (Becerra et al., 2011; Lu et al., 2012). Hippocampus and thalamus are also regions that are highly affected by neuronal degeneration in the IPKA rat model (Bertoglio et al., 2017; Sharma et al., 2008).

Table 3
Results of statistical analysis of number of transitions between states of functional connectivity and functional network topology, *p*-values are FDR-corrected for multiple comparisons.

Number of transitions		Effect of group		Effect of time IPKA group		Effect of time control group	
States of functional connectivity	Total	$U = 1.64\ 10^3$	$p = .016$	$X^2 = 17.2$	$p = .005$	$X^2 = 8.03$	$p = .465$
	Between states 1&2	$U = 1.29\ 10^3$	$p < .001$	$X^2 = 30.2$	$p < .001$	$X^2 = 4.22$	$p = 1.00$
	Between states 2&3	$U = 1.23\ 10^3$	$p < .001$	$X^2 = 38.3$	$p < .001$	$X^2 = 3.79$	$p = .870$
	Between states 3&4	$F_{1,25.3} = 11.2$	$p = .005$	$F_{5,124} = 9.08$	$p < .001$	$F_{5,123} = 2.38$	$p = .252$
	Between states 4&5	$F_{1,26.1} = 1.56$	$p = .222$	$F_{5,125} = 2.81$	$p = .019$	$F_{5,123} = 0.529$	$p = .754$
	Between states 5&6	$U = 3.27\ 10^3$	$p < .001$	$X^2 = 32.5$	$p < .001$	$X^2 = 2.97$	$p = .846$
States of functional network topology	Total	$U = 1.54\ 10^3$	$p = .006$	$X^2 = 9.32$	$p = .116$	$X^2 = 4.71$	$p = 1.00$
	Between states 1&2	$U = 1.46\ 10^3$	$p < .001$	$X^2 = 31.8$	$p < .001$	$X^2 = 1.79$	$p = .877$
	Between states 2&3	$U = 1.12\ 10^3$	$p < .001$	$X^2 = 31.9$	$p < .001$	$X^2 = 1.90$	$p = 1.00$
	Between states 3&4	$U = 1.26\ 10^3$	$p < .001$	$X^2 = 34.7$	$p < .001$	$X^2 = 6.40$	$p = 1.00$
	Between states 4&5	$F_{1,25.0} = 0.264$	$p = .612$	$F_{5,122} = 1.53$	$p = .185$	$F_{5,122} = 0.665$	$p = 1.00$
	Between states 5&6	$U = 1.07\ 10^3$	$p < .001$	$X^2 = 28.3$	$p < .001$	$X^2 = 3.08$	$p = 1.00$

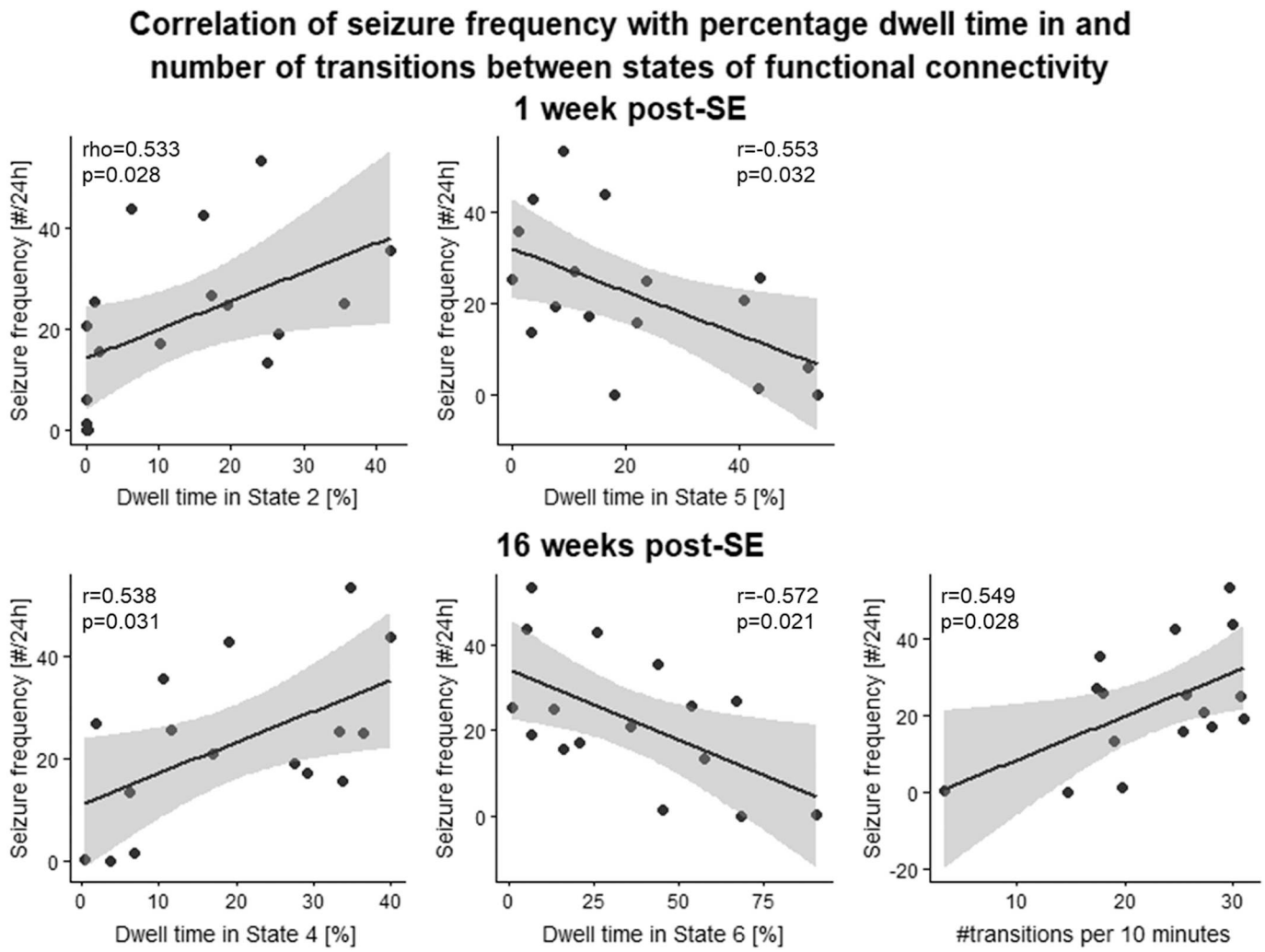

Fig. 9. Correlation between average daily seizure frequency (number per 24 h) on the one hand and percentage dwell time in and total number of transitions per scan between states of functional connectivity 1 week and 16 weeks post-SE on the other hand.

4.2. Changes in variability of functional connectivity, segregation and integration

Furthermore, our study indicates that the total number of transitions between states of functional connectivity and network topology is lower in the IPKA group compared to the control group, i.e., the flexibility is lower. Variability in functional connectivity and integration, assessed using the standard deviation over scanning time of network metrics, was lower in the IPKA animals compared to the control group, while variability in segregation was higher. This is in line with the findings of Douw et al. (2015), who found a lower flexibility in functional connectivity of the posterior cingulate cortex in patients with

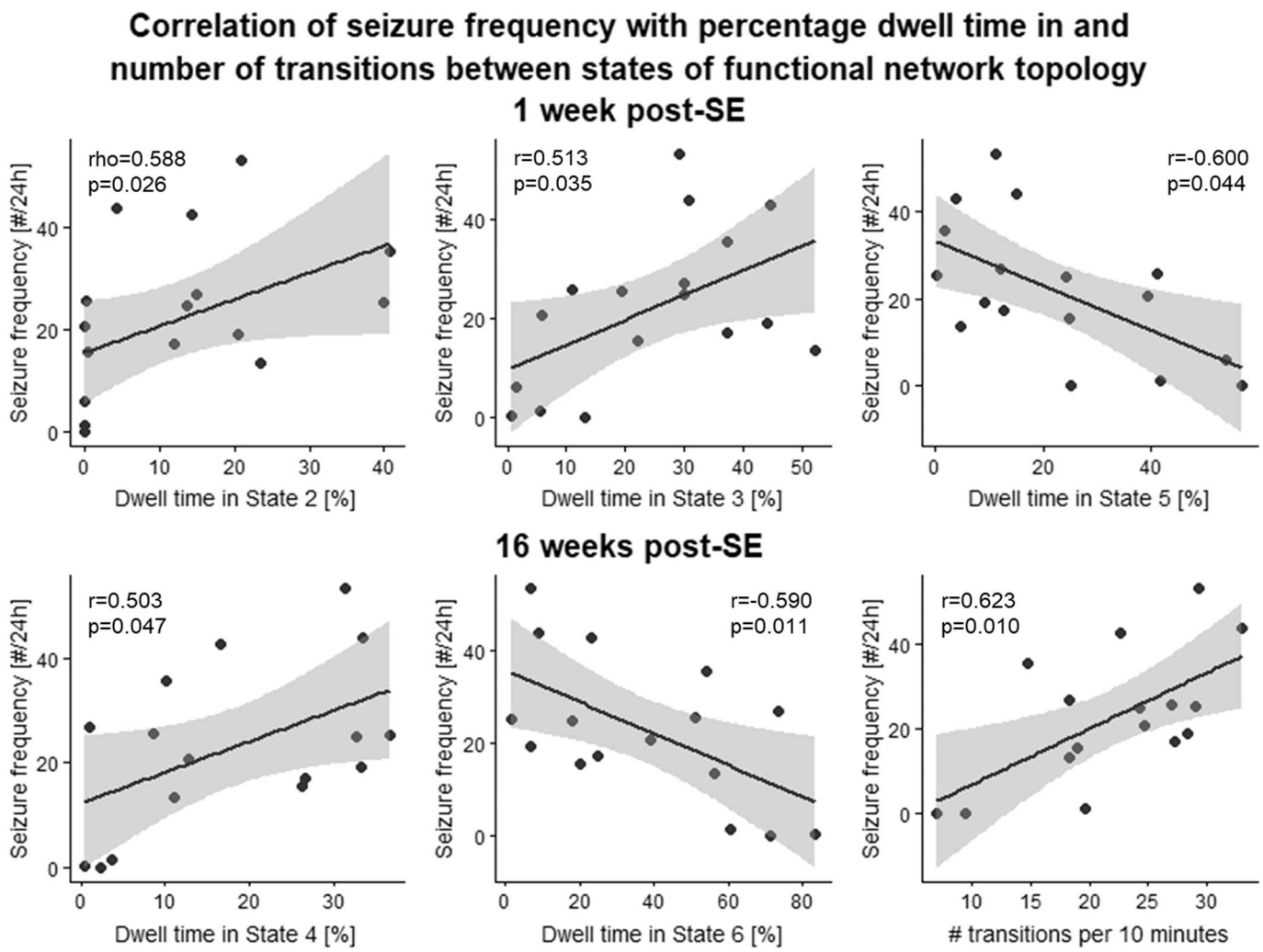

Fig. 10. Correlation between average daily seizure frequency (number per 24 h) on the one hand and percentage dwell time in and total number of transitions per scan between states of functional network topology 1 week and 16 weeks post-SE on the other hand.

Table 4
Results of two-sample Kolmogorov-Smirnov test to assess whether percentage dwell time and number of transitions differed significantly between the IPKA group 16 weeks post-SE and the validation group 20 weeks post-SE.

	State 1	State 2	State 3	State 4	State 5	State 6	Number of transitions
Z	0.686	0.610	0.324	0.175	0.583	0.058	0.262
p	0.493	0.542	0.746	0.861	0.560	0.954	0.793

TLE, which was correlated with disturbed memory functioning.

Since the FC states mostly differ in mean value rather than specific connections or ROIs and transitions predominantly occur between neighbouring states, it is possible that there is a continuum between states and our classification is somewhat artificial. However, even if this would be the underlying truth, our main conclusions still stand, namely that functional connectivity, integration and segregation are more often low and vary less in IPKA animals compared to control animals and that animals that dwell in states of high FC, have more chronic seizures.

4.3. Correlation with seizure frequency

Interestingly, average daily seizure frequency was positively correlated with percentage dwell time in states with a high mean functional connectivity and high segregation and integration, and negatively with dwell time in states with a low mean functional connectivity and low segregation and integration, 1 and 16 weeks post-SE. So, our findings indicate that animals that dwell in states with high functional connectivity, segregation and integration have more chronic seizures. This is in line with the findings of Bertoglio et al. (2019), who reported a positive correlation between functional brain connectivity and seizure frequency in the IPKA model for TLE. On the other hand, residing in states of low functional connectivity, associated with lower seizure frequencies, may reflect the protective effect and effectiveness of the treatment of epilepsy by means of resective/disconnective surgery (Englot et al., 2017). Since FC is more restricted to the states with the lowest FC, integration and segregation in animals that have fewer seizures, it is conceivable that temporary increases in FC might be necessary for seizures to be generated.

We also found a positive correlation between number of seizures on the one hand and the number of transitions 16 weeks post-SE and standard deviation over scanning time of global degree and local efficiency 1 week post-SE on the other hand, indicating that number of seizures is higher in animals with more variable functional connectivity.

4.4. Dynamic functional connectivity in patients with TLE

In the last five years, several studies investigated dFC in patients with TLE. Laufs et al. (2014) found that the BOLD signal variance was increased in the temporal pole, including the hippocampus, and

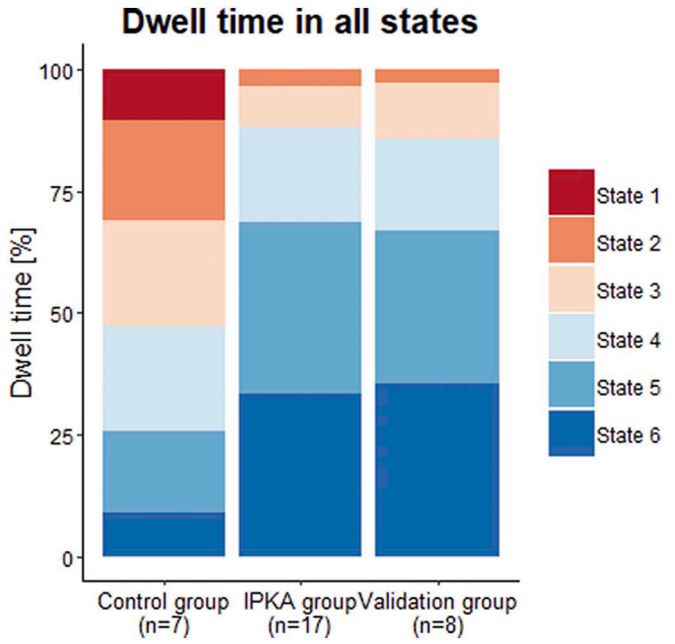

Fig. 11. Percentage dwell time in each state for the control group and IPKA group 16 weeks post-SE and the validation group 20 weeks post-SE. Data are visualized as a stacked bar graph with mean values.

reported greater variance in dFC between this brain region and the precuneus, sensory motor structures and frontal cortices using seed-based correlation and a sliding window analysis. Morgan et al. (2015) calculated the standard deviation across 20 FC values of a network, obtained using a sliding window approach, and covariance of the FC time series between two networks and found a nonsignificant decrease in FC in the cingulate midline network in TLE patients and an increase in FC variability that was correlated with disease duration (Morgan et al., 2015). Using a Bayesian hidden Markov model approach, Chiang et al. (2016) found that small-world index was more stationary than characteristic path length in TLE patients, but less than clustering coefficient, suggesting that the balance between integration and segregation might be affected in these patients (Chiang et al., 2016). Two years later, Chiang et al. (2018) found decreased FC and several abnormal spectral features of FC between the DMN and the memory network in TLE patients, that indicated that FC fluctuated at lower frequencies and with less variability, using a Generalized Autoregressive Conditional Heteroskedasticity model and time-frequency analysis. They reported that this may lead to a lower flexibility for cognitive processing, which could be related to the memory impairment that is often seen in TLE patients (Chiang et al., 2018). Overall, these studies found that FC variability was both increased, which was correlated with disease duration, and decreased, which was related to impaired cognitive processing. This is in line with our results, which show that variability in FC is lower in IPKA animals, but a higher variability is related to a higher seizure frequency.

4.5. Validation data set

We believe that this is the first study investigating dynamic functional connectivity in a rat model of epilepsy. To validate our findings, we repeated the analysis for a different data set consisting of rsfMRI scans of 8 IPKA animals acquired 20 weeks post-SE. Percentage dwell time in each state and the number of transitions in the validation data set were very similar to the ones in the IPKA group of the main data set 16 weeks post-SE, and statistically indistinguishable.

4.6. Limitations

To make sure that the fluctuations in FC are related to brain functions and are not artifacts, it is important to choose appropriate parameters, such as window length, and to use the right statistical tests (Preti et al., 2017). We chose a window length based on the recommendations in literature and repeated our analysis using a longer and shorter window length, which led to similar results. Our dFC findings are also in line with previous findings using static FC analysis. Therefore, we believe that the fluctuations in FC we found, are related to underlying brain activity.

While we found clear differences in dynamic functional connectivity and network topology between IPKA animals and control animals, it is not easy to link them directly to specific mechanisms of epileptogenesis. It is clear that the timeline of our findings corresponds well with known structural changes in the IPKA model, such as neuronal degeneration and gliosis, which suggests that these are most likely related. Other imaging techniques, such as diffusion MR imaging, might help to elucidate the relationship between changes in (dynamic) functional connectivity and mechanisms of epileptogenesis.

4.7. Future work

We found a lower flexibility in FC, which might be related to cognitive problems and memory impairment (Preti et al., 2017). In future studies we aim to confirm this with behavioural testing. In addition, we would like to investigate changes in structural connectivity underlying alterations in (dynamic) functional connectivity. We believe this will improve the understanding of how altered functional connectivity is related to structural lesions during epileptogenesis. Therefore, we plan to do a longitudinal rsfMRI and diffusion MRI study, combined with behavioural testing.

5. Conclusion

We investigated changes in dynamic functional connectivity and network topology during epileptogenesis in the IPKA rat model of TLE using longitudinal resting state fMRI. First, we found that functional connectivity states with a lower mean functional connectivity and network topologies with a lower segregation and integration occur more often in IPKA animals compared to control animals. In addition, functional connectivity becomes less variable during epileptogenesis. Secondly, we found a positive correlation of average daily seizure frequency with percentage dwell time in states with a high mean functional connectivity, high segregation and integration, and a higher number of transitions, and a negative correlation with percentage dwell time in states with a low mean functional connectivity and low segregation and integration. This indicates that animals that dwell in states of higher functional connectivity, segregation, integration, and have a higher FC variability, have more chronic seizures.

Declaration of Competing Interest

This research was financially supported by a PhD grant from the Special Research Fund (BOF) of Ghent University. Emma Christiaen and Marie-Gabrielle Goossens are SB PhD fellows at Research Foundation – Flanders (project numbers 1S90218N and 1S30017N). The authors have no competing interests to declare.

Acknowledgements

The authors would like to thank Yi Li for exploring the possibilities of dynamic functional connectivity during his master thesis.

Appendix A. Influence of window length

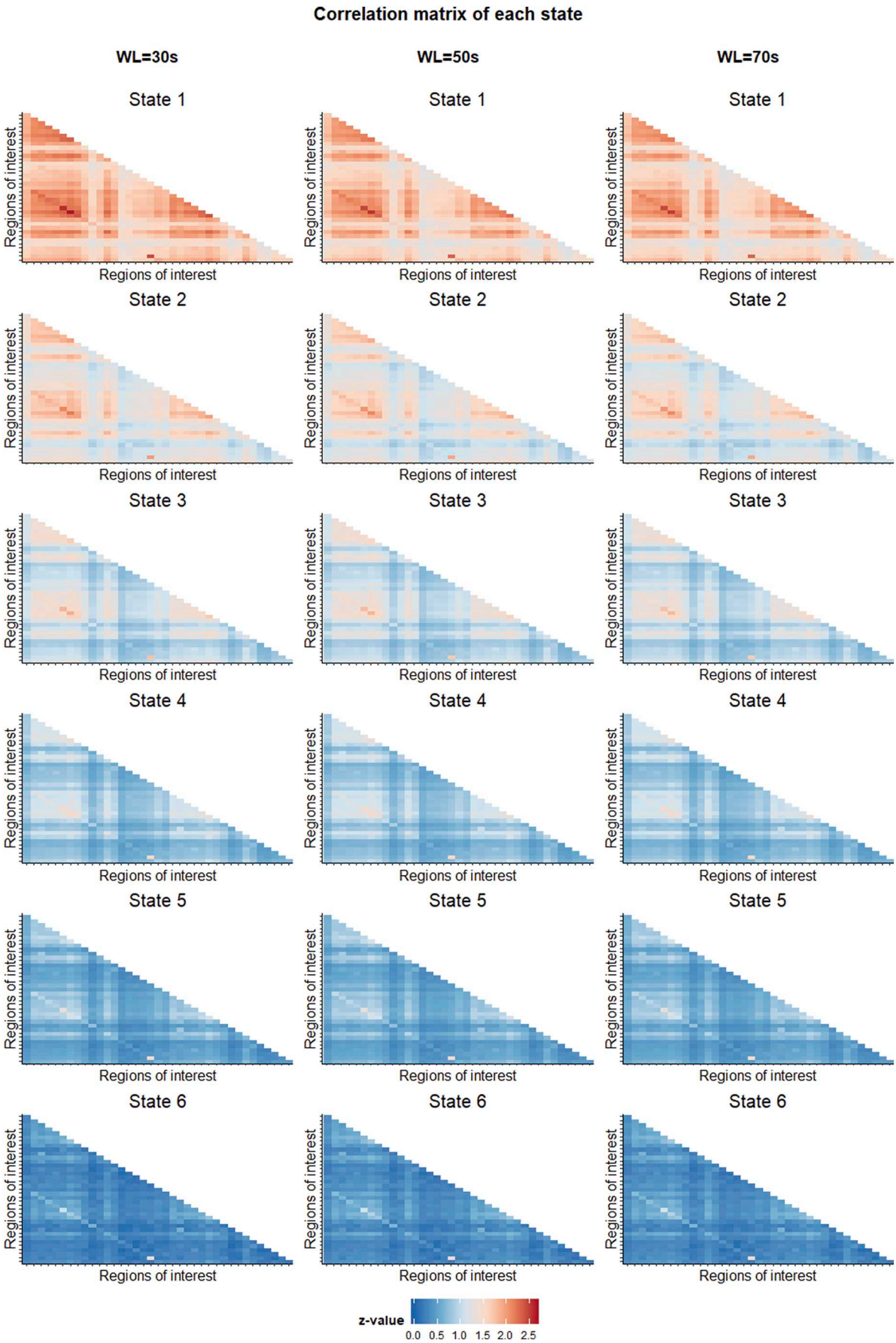

Fig. A.1. Correlation matrices (z-score) of 6 recurring states of functional connectivity, sorted from highest (State 1) to lowest (State 6) mean value for each window length.

Table A.1
Characterization of each state for each window length.

	Window length	State 1	State 2	State 3	State 4	State 5	State 6
Mean	30 s	1.75	1.35	1.06	0.810	0.566	0.304
	50 s	1.65	1.28	1.03	0.798	0.580	0.350
	70 s	1.63	1.25	1.01	0.782	0.574	0.354
Standard deviation	30 s	0.244	0.242	0.231	0.212	0.185	0.139
	50 s	0.241	0.238	0.224	0.206	0.178	0.144
	70 s	0.241	0.235	0.222	0.204	0.174	0.144
Maximum	30 s	2.64	2.18	1.86	1.57	1.43	1.35
	50 s	2.53	2.11	1.81	1.55	1.42	1.35
	70 s	2.50	2.09	1.78	1.53	1.42	1.35
Minimum	30 s	1.22	0.859	0.623	0.419	0.233	0.056
	50 s	1.13	0.800	0.612	0.425	0.264	0.081
	70 s	1.12	0.782	0.594	0.416	0.263	0.086

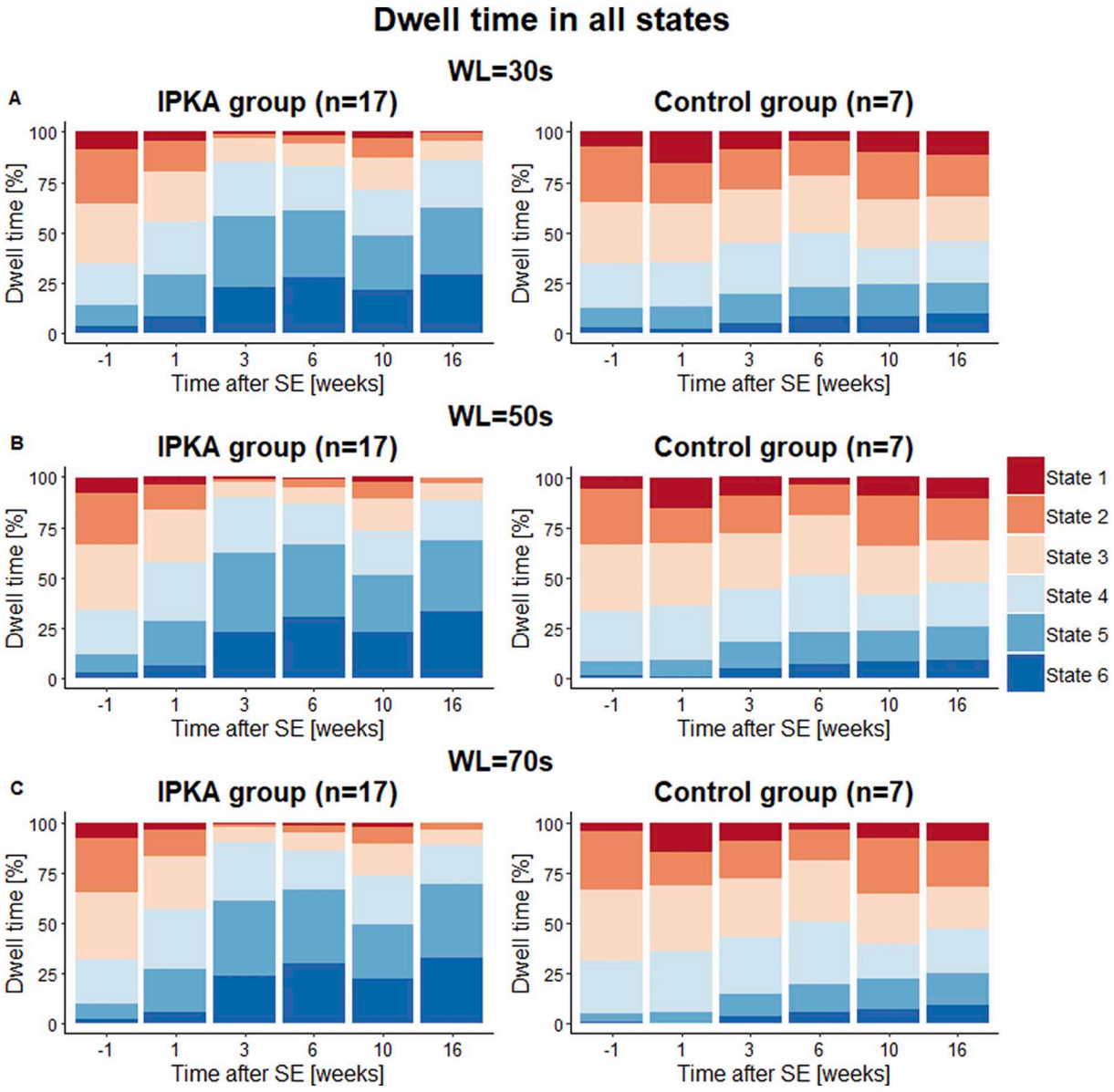

Fig. A.2. Percentage dwell time in each state for different window lengths. Data are visualized as a stacked bar graph with mean values.

Table A.2
Results of statistical analysis of percentage dwell time (%DT) and number of transitions using LMEM, p-values are FDR-corrected for multiple comparisons.

	Window length	Effect of group		Effect of time IPKA group		Effect of time control group	
%DT in State 1	30 s	$U = 1.24\ 10^3$	$p < .001$	$X^2 = 27.4$	$p < .001$	$X^2 = 3.02$	$p = .836$
	50 s	$U = 1.29\ 10^3$	$p < .001$	$X^2 = 28.5$	$p < .001$	$X^2 = 3.39$	$p = .768$
	70 s	$U = 1.54\ 10^3$	$p < .001$	$X^2 = 31.1$	$p < .001$	$X^2 = 3.89$	$p = .679$
%DT in State 2	30 s	$U = 1.24\ 10^3$	$p < .001$	$X^2 = 33.9$	$p < .001$	$X^2 = 2.09$	$p = .837$
	50 s	$U = 1.20\ 10^3$	$p < .001$	$X^2 = 36.1$	$p < .001$	$X^2 = 3.96$	$p = 1.00$
	70 s	$U = 1.27\ 10^3$	$p < .001$	$X^2 = 38.2$	$p < .001$	$X^2 = 3.21$	$p = .668$
%DT in State 3	30 s	$F_{1,26.3} = 14.1$	$p = .001$	$F_{5,125} = 17.2$	$p < .001$	$F_{5,123} = 0.988$	$p = 1.00$
	50 s	$F_{1,26.0} = 14.6$	$p = .001$	$F_{5,125} = 17.7$	$p < .001$	$F_{5,123} = 1.22$	$p = 1.00$
	70 s	$F_{1,25.8} = 16.2$	$p < .001$	$F_{5,125} = 16.0$	$p < .001$	$F_{5,123} = 1.44$	$p = 1.00$
%DT in State 4	30 s	$F_{1,25.7} = 0.200$	$p = .658$	$F_{5,124} = 1.71$	$p = .137$	$F_{5,122} = 0.973$	$p = 1.00$
	50 s	$U = 8.24\ 10^3$	$p = .724$	$X^2 = 11.1$	$p = .050$	$X^2 = 5.78$	$p = .987$
	70 s	$U = 2.06\ 10^3$	$p = .479$	$X^2 = 10.0$	$p = .074$	$X^2 = 6.11$	$p = .880$
%DT in State 5	30 s	$F_{1,26.4} = 17.2$	$p < .001$	$F_{5,124} = 23.6$	$p < .001$	$F_{5,123} = 0.660$	$p = .983$
	50 s	$F_{1,26.0} = 16.9$	$p = .001$	$F_{5,124} = 16.9$	$p < .001$	$F_{5,123} = 0.780$	$p = .849$
	70 s	$F_{1,25.9} = 17.5$	$p < .001$	$F_{5,125} = 14.9$	$p < .001$	$F_{5,123} = 0.992$	$p = .850$
%DT in State 6	30 s	$U = 3.23\ 10^3$	$p < .001$	$X^2 = 35.7$	$p < .001$	$X^2 = 3.60$	$p = 1.00$
	50 s	$U = 8.90\ 10^3$	$p < .001$	$X^2 = 37.5$	$p < .001$	$X^2 = 2.57$	$p = .766$
	70 s	$U = 3.35\ 10^3$	$p < .001$	$X^2 = 35.7$	$p < .001$	$X^2 = 4.61$	$p = .698$
Number of transitions	30 s	$U = 2.22\ 10^3$	$p = .969$	$X^2 = 6.59$	$p = .253$	$X^2 = 2.35$	$p = .799$
	50 s	$U = 1.64\ 10^3$	$p = .013$	$X^2 = 17.2$	$p = .004$	$X^2 = 8.03$	$p = .155$
	70 s	$U = 2.97\ 10^3$	$p = .002$	$X^2 = 12.2$	$p = .032$	$X^2 = 5.96$	$p = .310$

Table A.3
Results of statistical analysis of correlation between percentage dwell time (%DT) and number of transitions per scan 1 week and 16 weeks post-SE, and average daily seizure frequency (number per 24 h). P-values are FDR-corrected for multiple comparisons.

			Correlation with seizure frequency		
			30 s	50 s	70 s
1 week post-SE	*%DT in State 2*	Pearson's r	0.513		
		Spearman's rho		0.533	0.532
		p	0.047	0.028	0.028
	%DT in State 5	Pearson's r	−0.585	−0.553	
		p	0.028	0.032	
	%DT in State 6	Spearman's rho	−0.491		
		p	0.045		
16 weeks post-SE	*%DT in State 4*	Pearson's r	0.528	0.538	0.540
		p	0.035	0.031	0.031
	%DT in State 6	Pearson's r	−0.591	−0.572	−0.571
		p	0.016	0.021	0.021
	Number of transitions	Pearson's r		0.549	
		p		0.028	

References

Battiston, F., Guillon, J., Chavez, M., Latora, V., De Vico Fallani, F., 2018. Multiplex core-periphery organization of the human connectome. J. R. Soc. Interface 15. https://doi.org/10.1098/rsif.2018.0514.

Becerra, L., Pendse, G., Chang, P.-C., Bishop, J., Borsook, D., 2011. Robust reproducible resting state networks in the awake rodent brain. PLoS One 6, e25701. https://doi.org/10.1371/journal.pone.0025701.

Bertoglio, D., Amhaoul, H., Van Eetveldt, A., Houbrechts, R., Van De Vijver, S., Ali, I., Dedeurwaerdere, S., 2017. Kainic acid-induced post-status Epilepticus models of temporal lobe epilepsy with diverging seizure phenotype and neuropathology. Front. Neurol. 8, 588. https://doi.org/10.3389/fneur.2017.00588.

Bertoglio, D., Jonckers, E., Ali, I., Verhoye, M., Van der Linden, A., Dedeurwaerdere, S., 2019. In vivo measurement of brain network connectivity reflects progression and intrinsic disease severity in a model of temporal lobe epilepsy. Neurobiol. Dis. 127, 45–52. https://doi.org/10.1016/J.NBD.2019.02.012.

Chang, C., Glover, G.H., 2010. Time–frequency dynamics of resting-state brain connectivity measured with fMRI. Neuroimage 50, 81–98. https://doi.org/10.1016/J.NEUROIMAGE.2009.12.011.

Chiang, S., Cassese, A., Guindani, M., Vannucci, M., Yeh, H.J., Haneef, Z., Stern, J.M., 2016. Time-dependence of graph theory metrics in functional connectivity analysis. Neuroimage 125, 601–615. https://doi.org/10.1016/j.neuroimage.2015.10.070.

Chiang, S., Vankov, E.R., Yeh, H.J., Guindani, M., Vannucci, M., Haneef, Z., Stern, J.M., 2018. Temporal and spectral characteristics of dynamic functional connectivity between resting-state networks reveal information beyond static connectivity. PLoS One 13, e0190220. https://doi.org/10.1371/journal.pone.0190220.

Christiaen, E., Goossens, M.-G., Raedt, R., Descamps, B., Larsen, L.E., Craey, E., Carrette, E., Vonck, K., Boon, P., Vanhove, C., 2019. Alterations in the functional brain network in a rat model of epileptogenesis: a longitudinal resting state fMRI study. Neuroimage 202, 116144. https://doi.org/10.1016/J.NEUROIMAGE.2019.116144.

Douw, L., Leveroni, C.L., Tanaka, N., Emerton, B.C., Cole, A.C., Reinsberger, C., Stufflebeam, S.M., 2015. Loss of resting-state posterior cingulate flexibility is associated with memory disturbance in left temporal lobe epilepsy. PLoS One 10, e0131209. https://doi.org/10.1371/journal.pone.0131209.

Engel Jr., J., 2014. Approaches to refractory epilepsy. Ann. Indian Acad. Neurol. 17, S12–S17. https://doi.org/10.4103/0972-2327.128644.

Englot, D.J., Birk, H., Chang, E.F., 2017. Seizure outcomes in nonresective epilepsy surgery: an update. Neurosurg. Rev. https://doi.org/10.1007/s10143-016-0725-8.

Fisher, R.S., Boas, W., van, E., Blume, W., Elger, C., Genton, P., Lee, P., Engel, J., 2005. Epileptic seizures and epilepsy: definitions proposed by the international league against epilepsy (ILAE) and the International Bureau for Epilepsy (IBE). Epilepsia 46, 470–472. https://doi.org/10.1111/j.0013-9580.2005.66104.x.

Fox, M.D., Greicius, M., 2010. Clinical applications of resting state functional connectivity. Front. Syst. Neurosci. 4, 19. https://doi.org/10.3389/fnsys.2010.00019.

Gill, R.S., Mirsattari, S.M., Leung, L.S., 2017. Resting state functional network disruptions in a kainic acid model of temporal lobe epilepsy. NeuroImage. Clin. 13, 70–81. https://doi.org/10.1016/j.nicl.2016.11.002.

Goldberg, E.M., Coulter, D.A., 2013. Mechanisms of epileptogenesis: a convergence on neural circuit dysfunction. Nat. Rev. Neurosci. 14, 337–349. https://doi.org/10.1038/nrn3482.

Grandjean, J., Preti, M.G., Bolton, T.A.W., Buerge, M., Seifritz, E., Pryce, C.R., Van De Ville, D., Rudin, M., 2017. Dynamic reorganization of intrinsic functional networks in the mouse brain. Neuroimage 152, 497–508. https://doi.org/10.1016/J.

NEUROIMAGE.2017.03.026.
Hellier, J.L., Patrylo, P.R., Buckmaster, P.S., Dudek, F.E., 1998. Recurrent spontaneous motor seizures after repeated low-dose systemic treatment with kainate: assessment of a rat model of temporal lobe epilepsy. Epilepsy Res. 31, 73–84.
Hutchison, R.M., Womelsdorf, T., Allen, E.A., Bandettini, P.A., Calhoun, V.D., Corbetta, M., Della Penna, S., Duyn, J.H., Glover, G.H., Gonzalez-Castillo, J., Handwerker, D.A., Keilholz, S., Kiviniemi, V., Leopold, D.A., de Pasquale, F., Sporns, O., Walter, M., Chang, C., 2013. Dynamic functional connectivity: promise, issues, and interpretations. Neuroimage 80, 360–378. https://doi.org/10.1016/J.NEUROIMAGE.2013.05.079.
Jiang, Y., Han, C.-L., Liu, H.-G., Wang, X., Zhang, X., Meng, F.-G., Zhang, J.-G., 2018. Abnormal hippocampal functional network and related memory impairment in pilocarpine-treated rats. Epilepsia 59, 1785–1795. https://doi.org/10.1111/epi.14523.
Ketchen, D.J., Shook, C.L., 1996. The application of cluster analysis in strategic management research: an analysis and critique. Strateg. Manag. J. 17, 441–458. https://doi.org/10.1002/(SICI)1097-0266(199606)17:6<441::AID-SMJ819>3.0.CO;2-G.
Klugah-Brown, B., Luo, C., He, H., Jiang, S., Armah, G.K., Wu, Y., Li, J., Yin, W., Yao, D., 2019. Altered dynamic functional network connectivity in frontal lobe epilepsy. Brain Topogr. 32, 394–404. https://doi.org/10.1007/s10548-018-0678-z.
Laufs, H., Rodionov, R., Thornton, R., Duncan, J.S., Lemieux, L., Tagliazucchi, E., 2014. Altered fMRI connectivity dynamics in temporal lobe epilepsy might explain seizure semiology. Front. Neurol. 5, 175. https://doi.org/10.3389/fneur.2014.00175.
Li, R., Liao, W., Yu, Y., Chen, Heng, Guo, X., Tang, Y.-L., Chen, Huafu, 2018a. Differential patterns of dynamic functional connectivity variability of striato-cortical circuitry in children with benign epilepsy with centrotemporal spikes. Hum. Brain Mapp. 39, 1207–1217. https://doi.org/10.1002/hbm.23910.
Li, R., Wang, L., Chen, Heng, Guo, X., Liao, W., Tang, Y.-L., Chen, Huafu, 2018b. Abnormal dynamics of functional connectivity density in children with benign epilepsy with centrotemporal spikes. Brain Imaging Behav. https://doi.org/10.1007/s11682-018-9914-0.
Liu, F., Wang, Y., Li, M., Wang, W., Li, R., Zhang, Z., Lu, G., Chen, H., 2017. Dynamic functional network connectivity in idiopathic generalized epilepsy with generalized tonic-clonic seizure. Hum. Brain Mapp. 38, 957–973. https://doi.org/10.1002/hbm.23430.
Lu, H., Zou, Q., Gu, H., Raichle, M.E., Stein, E.A., Yang, Y., 2012. Rat brains also have a default mode network. Proc. Natl. Acad. Sci. U. S. A. 109, 3979–3984. https://doi.org/10.1073/pnas.1200506109.
Matthews, P.M., Jezzard, P., 2004. Functional magnetic resonance imaging. J. Neurol. Neurosurg. Psychiatry 75, 6–12.
Morgan, V.L., Abou-Khalil, B., Rogers, B.P., 2015. Evolution of functional connectivity of brain networks and their dynamic interaction in temporal lobe epilepsy. Brain Connect. 5, 35–44. https://doi.org/10.1089/brain.2014.0251.
Paxinos, G., Watson, C., 2013. The Rat Brain in Stereotaxic Coordinates: Hard Cover Edition. Elsevier Science.
Pedersen, M., Omidvarnia, A., Curwood, E.K., Walz, J.M., Rayner, G., Jackson, G.D., 2017. The dynamics of functional connectivity in neocortical focal epilepsy. NeuroImage Clin. 15, 209–214. https://doi.org/10.1016/J.NICL.2017.04.005.
Pirttimäki, T., Salo, R.A., Shatillo, A., Kettunen, M.I., Paasonen, J., Sierra, A., Jokivarsi, K., Leinonen, V., Andrade, P., Quittek, S., Pitkänen, A., Gröhn, O., 2016. Implantable RF-coil with multiple electrodes for long-term EEG-fMRI monitoring in rodents. J. Neurosci. Methods 274, 154–163. https://doi.org/10.1016/j.jneumeth.2016.10.014.
Preti, M.G., Bolton, T.A., Van De Ville, D., 2017. The dynamic functional connectome: state-of-the-art and perspectives. Neuroimage 160, 41–54. https://doi.org/10.1016/J.NEUROIMAGE.2016.12.061.
Rubinov, M., Sporns, O., 2010. Complex network measures of brain connectivity : uses and interpretations. Neuroimage 52, 1059–1069. https://doi.org/10.1016/j.neuroimage.2009.10.003.
Sharma, A.K., Jordan, W.H., Reams, R.Y., Hall, D.G., Snyder, P.W., 2008. Temporal profile of clinical signs and Histopathologic changes in an F-344 rat model of Kainic acid–induced mesial temporal lobe epilepsy. Toxicol. Pathol. 36, 932–943. https://doi.org/10.1177/0192623308326093.
Smitha, K.A., Akhil Raja, K., Arun, K.M., Rajesh, P.G., Thomas, B., Kapilamoorthy, T.R., Kesavadas, C., 2017. Resting state fMRI: a review on methods in resting state connectivity analysis and resting state networks. Neuroradiol. J. 30, 305–317. https://doi.org/10.1177/1971400917697342.
Wang, J., Zuo, X., He, Y., 2010. Graph-based network analysis of resting-state functional MRI. Front. Syst. Neurosci. 4, 16. https://doi.org/10.3389/fnsys.2010.00016.
Wang, J., Wang, X., Xia, M., Liao, X., Evans, A., He, Y., 2015. GRETNA: a graph theoretical network analysis toolbox for imaging connectomics. Front. Hum. Neurosci. 9, 386. https://doi.org/10.3389/fnhum.2015.00386.
Wang, Y., Berglund, I.S., Uppman, M., Li, T.-Q., 2019. Juvenile myoclonic epilepsy has hyper dynamic functional connectivity in the dorsolateral frontal cortex. NeuroImage Clin. 21, 101604. https://doi.org/10.1016/j.nicl.2018.11.014.
Weber, R., Ramos-Cabrer, P., Wiedermann, D., van Camp, N., Hoehn, M., 2006. A fully noninvasive and robust experimental protocol for longitudinal fMRI studies in the rat. Neuroimage 29, 1303–1310. https://doi.org/10.1016/J.NEUROIMAGE.2005.08.028.